Cell Communication and Signaling

RESEARCH

Open Access

Inhibition of Farnesoid-x-receptor signaling during abdominal sepsis by dysbiosis exacerbates gut barrier dysfunction

Shuwen Qian[1,2,7*†], Zehua Su[2,7†], Jiaqi Lin[2,7], Qianhao Hou[2,7], Xiaomei Wang[2], Yuling Li[3], Jieying Wang[4], Changchun Huang[5], Zetian Wang[2,7], Francisco Javier Cubero[6], Xiangrui Wang[2,7*] and Lijun Liao[2,7*]

Abstract

Background and aims Bacterial translocation and intestinal dysbiosis due to gut barrier dysfunction are widely recognized as major causes of the initiation and development of intra-abdominal sepsis. Systemic bacterial translocation and hepatic activation of the myeloid differentiation primary response gene 88 (Myd88) can disturb bile acids (BAs) metabolism, further exacerbating intestinal dysbiosis. The farnesoid X receptor (FXR) and fibroblast growth factor (FGF) 15/19 are well known to be involved in the control of BAs synthesis and enterohepatic circulation. However, the influence of intestinal microbiota on intestinal Myd88 signaling, the FXR/FGF15 axis, as well as gut-liver crosstalk during sepsis remains unclear. The present study aims to decipher the role of intestinal Myd88 in abdominal sepsis, its impact on intestinal FXR signaling and FGF15-mediated gut-liver crosstalk.

Methods Expression levels of FXR and FGF15 in the liver and intestines, alongside assessments of gut barrier function, were evaluated in septic wild-type (WT) mice 24 h post-cecal ligation and puncture (CLP) surgery. Subsequently, the FXR agonist INT-747 was administered to explore the relationship between FXR activation and gut barrier function. Further investigations involved Myd88-deficient mice with specific deletion of Myd88 in intestinal epithelial cells ($Myd88^{\Delta IEC}$), subjected to CLP to examine the interplay among intestinal Myd88, FXR, gut barrier function, microbiota, and BA composition. Additionally, fecal microbiota transplantation (FMT) from septic mice to $Myd88^{\Delta IEC}$ mice was conducted to study the impact of dysbiosis on intestinal Myd88 expression during sepsis, using floxed ($Myd88^{fl/fl}$) mice as controls. Finally, the effects of the probiotic intervention on gut barrier function and sepsis outcomes in CLP mice were investigated.

Results Induction of sepsis via CLP led to hepatic cholestasis, suppressed FXR-FGF15 signaling, altered gut microbiota composition, and compromised gut barrier function. Administration of INT-747 increased intestinal FXR and FGF15 expression, strengthened gut barrier function, and enhanced barrier integrity. Interestingly, $Myd88^{\Delta IEC}$ mice exhibited partial reversal of sepsis-induced changes in FXR signaling, BA metabolism, and intestinal function, suggesting enhanced FXR expression upon Myd88 knockdown. Moreover, FMT from septic mice activated intestinal Myd88, subsequently suppressing FXR-FGF15 signaling, exacerbating cholestasis, and ultimately compromising gut

†Shuwen Qian and Zehua Su contributed equally to this work.

*Correspondence:
Shuwen Qian
shuwen_qian@tongji.edu.cn
Xiangrui Wang
xiangruiwang@vip.sina.com
Lijun Liao
liao@pan-intelligence.com
Full list of author information is available at the end of the article

© The Author(s) 2025. **Open Access** This article is licensed under a Creative Commons Attribution-NonCommercial-NoDerivatives 4.0 International License, which permits any non-commercial use, sharing, distribution and reproduction in any medium or format, as long as you give appropriate credit to the original author(s) and the source, provide a link to the Creative Commons licence, and indicate if you modified the licensed material. You do not have permission under this licence to share adapted material derived from this article or parts of it. The images or other third party material in this article are included in the article's Creative Commons licence, unless indicated otherwise in a credit line to the material. If material is not included in the article's Creative Commons licence and your intended use is not permitted by statutory regulation or exceeds the permitted use, you will need to obtain permission directly from the copyright holder. To view a copy of this licence, visit http://creativecommons.org/licenses/by-nc-nd/4.0/.

barrier function. Probiotic treatment during abdominal sepsis mitigated flora disturbances, reduced Myd88 activation in the intestinal epithelium, increased FXR expression, alleviated cholestasis, and consequently reduced barrier damage.

Conclusions This study highlights the critical role of Myd88/FXR signaling in intestinal epithelial cells as a pivotal mediator of the detrimental effects induced by sepsis-related intestinal dysbiosis on barrier function and bile acid metabolism. In summary, disordered intestinal flora in septic mice specifically triggers intestinal epithelial Myd88 activation, inhibit the FXR-FGF15 axis, and then worsen intestinal barrier function impairment.

Keywords Sepsis, Gut microbiota, Myd88, FXR, FGF15, Probiotics, Bile acids

Graphical Abstract

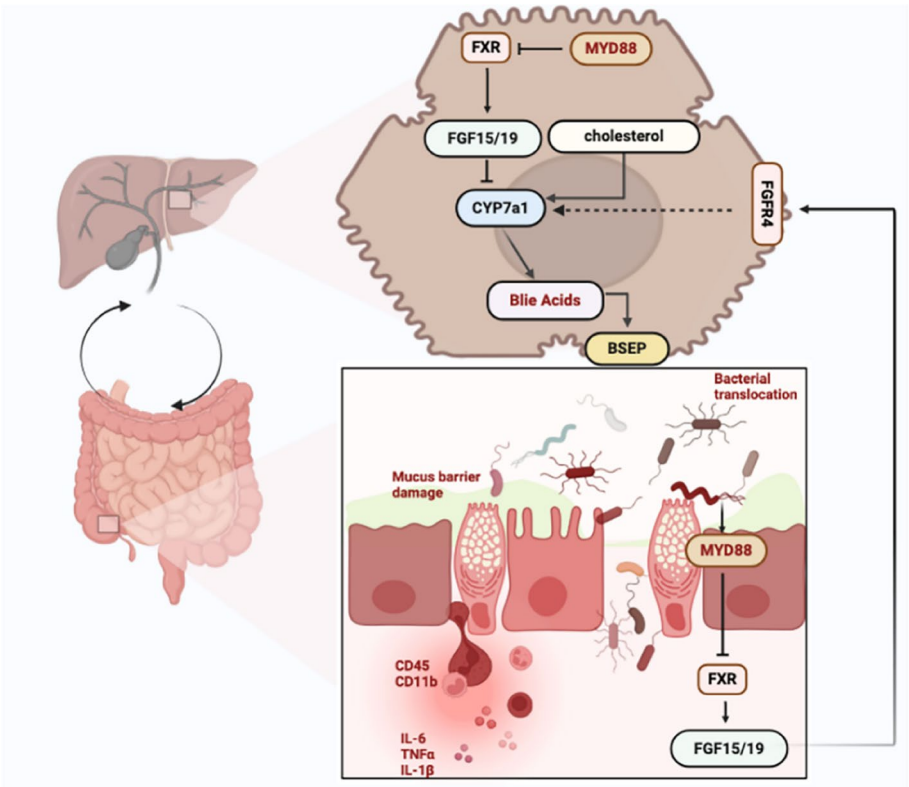

Introduction

Sepsis, a life-threatening condition resulting from a dysregulated host response to infection, remains a major challenge in critical care medicine [1]. The gut has long been recognized as the "motor" of critical illness [2]. Critical illness and acute injury may induce gut barrier dysfunction, characterized by intestinal hyperpermeability, dysbiosis, bacterial translocation, and immunosuppression. These changes can exacerbate sepsis progression and cause distant organ damage, including the intestine itself [2–4]. The intestine plays a pivotal role in the development of multiple organ dysfunction syndromes (MODS) [5, 6]. Therapeutic interventions aimed at enhancing intestinal function can significantly improve survival and outcomes in sepsis [7, 8]. The'gut-liver axis'is thought to play an important role in the pathogenesis of sepsis. This complex bidirectional communication system between the intestine and the liver is critical for maintaining metabolic homeostasis, and shaping the microbiome through bile acids (BAs) [9].

BAs are synthesized in the liver from cholesterol and play a crucial role in lipid digestion and absorption in the intestine [10]. They serve as signaling molecules by

activating the farnesoid X receptor (FXR) and subsequent inducing fibroblast growth factor 15 (FGF15 in mice; FGF19 in humans) in the intestine [11]. However, during sepsis, there is evidence of dysregulated BA metabolism, characterized by alterations in BA composition and impaired FXR-FGF15 signaling. Cholestasis is an independent risk factor for poor prognosis in patients with sepsis, as those with cholestasis have a significantly higher mortality rate compared to those without [12]. FXR, as one of the most common BA receptors, is mainly expressed in enterocytes of ileum mucosa and hepatocytes. Intestinal FXR activation induces the transcription of FGF15/19, which is delivered to the liver and binds to fibroblast growth factor receptor 4 (FGFR4). This initiates a signaling cascade that inhibits cytochrome CYP7 A1 expression, ultimately suppressing BAs synthesis [13, 14]. FXR is a crucial factor in regulating immunity within the gastrointestinal tract and exerts an anti-inflammatory role in DSS-induced colitis [15]. Intestinal microbiota metabolizes BAs in the intestine, altering their signaling via BAs receptors. FXR mRNA expression in the liver was found to be down-regulated as early as 8 h after lipopolysaccharide (LPS) administration in mice [16]. Additionally, in murine ileal specimens cultured in vitro, the FXR transcriptional activity was repressed by NF-kappaB signaling activated by inflammatory factors such as TNFα and IL-1β [17]. FXR remains a key component of the nuclear receptor network that regulates intestinal innate immunity and homeostasis in animal models of colitis [18].

The homeostasis of gut microbiota is crucial in the pathophysiology of sepsis. Research has indicated that diversity of gut microbial species significantly decreases within 6 h (h) of admission to the intensive care unit, correlating with a poor prognosis in critically ill patients [19]. In addition to nutrient extraction and synthesis, the intestinal microbiota plays a crucial role in absorbing nutrient metabolites and maintaining the integrity of the intestinal epithelium. This is achieved through the secretion of antimicrobial metabolites that combat pathogenic bacteria and regulate immune cell function [20]. In patients with abdominal sepsis, gut microbiota homeostasis plays a vital role in the maintenance of the intestinal barrier. Dysbiosis or imbalance in gut flora can cause endotoxin to pass from the gut lumen to the outer intestinal wall, leading to mucosal immune dysfunction, structural impairment of the intestine, and barrier function loss [21].

Myd88 (Myeloid differentiation primary response gene 88) is an adaptor protein that plays a crucial role in mediating the innate immune response upon recognition of danger-associated molecular patterns (DAMPs) and pathogen-associated molecular patterns (PAMPs) [22]. Myd88 is closely related to sepsis and intestinal microbiota. The Myd88-Ticam1 pathway is responsible for the production of REGIII, an antimicrobial peptide, which can modulate the composition and abundance of the intestinal microbiota [23]. Meanwhile, flagellated intestinal commensal bacteria can synergize with Myd88 and contribute to the reduction of intestinal infections (e.g., Cryptosporidium parvum) [24]. Moreover, Clostridium butyricum can improve intestinal function by enhancing TLR2-Myd88-NF-κB signaling [25]. Furthermore, FXR gene expression and function in the intestine are modulated by Toll-like receptors (TLRs). TLR9/Myd88/IRF7 signaling positively regulates FXR expression in the intestine, and FXR mediates housekeeping activities of TLR9, thus linking microbiota-sensing receptors to immune and metabolic signaling in the intestine [26]. TLRs and Myd88 are critically linked with several metabolic pathways, including BAs metabolism and inflammation [27]. However, the specific role of intestinal epithelial Myd88 in the relationship between BA metabolism and intestinal inflammation remains elusive.

Dysbiosis, characterized by the overgrowth of pathogenic bacteria and reduction of beneficial commensals, further contributes to BA dysregulation and liver injury in septic patients. Understanding the intricate interplay between sepsis, hepatic injury, BA metabolism, and the gut-liver axis is essential for the development of novel therapeutic strategies aimed at mitigating the adverse effects of sepsis on intestinal function and improving patient outcomes.

The aim of this study was to investigate the role of intestinal epithelial Myd88 in the FXR-FGF15 axis and its impact on intestinal barrier function in sepsis, as well as the role of intestinal flora and its underlying mechanisms.

Results

Abnormal liver function, cholestasis and intestinal damage following sepsis may be linked to metabolic imbalances in the enterohepatic axis involving FXR

The murine model of peritoneal, polymicrobial sepsis, known as cecal ligation and puncture (CLP), is widely acknowledged as the gold standard experimental model and is highly analogous to human sepsis [28]. Notably, the severity of the model can be modulated by alterations in the location, number, and size of the punctures. In this study, we adopted the standardized CLP procedure as described by Rittirsch [29]. The acute mortality of this model was considerable, which was conducive to investigating the effects of interventions on the sepsis model. Proficiency in this procedure by the same operator is essential to guarantee consistency throughout the experiment.

At 24 h after CLP surgery, the survival rate for CLP mice was 65%, which declined to 50% at 48 h (Fig. 1A), in accordance with previous reports [30, 31]. Notably, 24 h after CLP surgery, liver lobules were impaired, showing vacuolar degeneration and infiltration of inflammatory cells, and the liver injury score escalated (Fig. 1B, C). These early time points (24–48 h) were selected to reflect the acute phase of sepsis, during which significant physiological and pathological changes occur, allowing us to evaluate the immediate therapeutic effects of the interventions. The significant elevation of total BAs (TBA) and alkaline phosphatase (AKP) serves as quintessential biomarkers of cholestatic pathology. The concurrent elevation of aspartate aminotransferase (AST) and alanine aminotransferase (ALT) suggests hepatic injury induced by sepsis. Moreover, elevated levels of serum IL-6 indicate a robust inflammatory response (Fig. 1D). These results suggested that the pathogenesis of sepsis might potentially be associated with bile metabolism.

To gain a deeper comprehension of BA metabolism during sepsis, we scrutinized the key intracellular regulators of BA synthesis and transport, FXR and FGF15. The regulators are known to inhibit BA synthesis and exert negative feedback on BA production. In sepsis, cholestasis and negative feedback might contribute to diminished expression of FXR and FGF15. In our study, both were found to be decreased in the hepatic tissue as indicated by immunohistochemistry (IHC) and western-blot (WB) (Fig. 1E, F). The adequate expression of bile salt export pump (BSEP) influences the flow and composition of bile. Here, in our result, BSEP expression in the liver was also reduced in sepsis (Fig. 1F). Given the intimate connection between the enterohepatic axis and intestinal damage in sepsis, we were intrigued to examine FXR and FGF15 expression in the ileum. The decreasing trend was consistent with that in the liver (Fig. 1G, H).

Cholestasis in sepsis prompted us to study FXR. We repeatedly confirmed that FXR and FGF15 are downregulated in the gut and liver during sepsis.

Sepsis-induced intestinal barrier disruption involves multiple factors, including epithelial, immune and microbiota barriers

Under normal circumstances, a dynamic equilibrium is sustained among three crucial elements: the intestinal epithelium, the microbiota, and the immune system. This balance is essential for maintaining gut homeostasis. However, in critical illness such as sepsis, this equilibrium is disrupted, leading to inflammation and dysfunction in distant organs. The intestinal barrier consists of several key components, including tight junction proteins like ZO-1, mucus primarily secreted by goblet cells (predominantly Muc2), and immune cell infiltration [5].

Twenty-four hours after cecal perforation, the entire gastrointestinal tract undergoes an inflammatory assault, with pathological damage observed in the ileum and colon. Hematoxylin and eosin (H&E) staining (Fig. 1G) and Alcian blue staining (Fig. 2A) revealed impaired intestinal structures, including villus atrophy and destruction, reduced goblet cell numbers, and increased crypt cell proliferation. IHC staining and Western blot analysis showed decreased expression of ZO-1, indicating disrupted continuity and impaired epithelial barrier function (Fig. 2B, C). Additionally, Muc2 secretion was significantly reduced in septic mice (Fig. 2B). IHC staining for CD45 and CD11b revealed extensive leukocyte and inflammatory cell infiltration in the ileum (Fig. 2C, D), highlighting the severe inflammatory response in the gut.

(See figure on next page.)

Fig. 1 Abnormal liver function, cholestasis, and intestinal damage following sepsis may be linked to metabolic imbalances in the enterohepatic axis involving FXR. **A** Comparison of 48 h survival rate between mice in the Sham and the CLP group. $n = 10$ per group. **B** Comparison of liver injury scores between the Sham group and the CLP group. $n = 6$ per group. **C** Comparison of liver and gallbladder gross specimens as well as HE staining of liver between the Sham group and the CLP group. HE staining of the liver indicated liver lobular damage and inflammatory infiltration in the CLP group. Scale bars represent 100 μm. **D** Serum TBAs, AKP, ALT, AST, and IL-6 levels at 24 h after CLP surgery in the Sham and CLP mice were detected by ELISA. $n = 6$ per group. **E** Immunohistochemistry staining and quantitative analysis revealed the expression of FXR and FGF15 was significantly reduced in the liver 24 h after CLP. 3 mice with 4 sections in each group were randomly measured. Scale bars represent 50 μm. **F** Protein abundance analysis of BSEP, FXR, and FGF15 was conducted by western blot in the liver. All measurements were normalized by using GAPDH expression as an internal standard. $n = 3$ per group. **G** Intestinal H&E staining and Chiu score of mice in Sham and CLP groups. $n = 6$ per group. Immunohistochemistry staining and quantitative analysis disclosed that the expression of FXR and FGF15 was significantly reduced in the intestine 24 h after CLP. 3 mice with 4 sections in each group were randomly measured. Scale bars represent 100 μm. **H** Protein abundance analysis of FXR and FGF15 was conducted by western blot in the intestine. All measurements were normalized by using GAPDH expression as an internal standard. $n = 3$ per group. All data were graphed as mean ± SEM and were considered statistically significant at $p < 0.05$ (*), $p < 0.01$ (**), $p < 0.001$ (***), and $p < 0.0001$ (****). Unpaired two-tailed t-tests were used, and the bars represent the mean and 95% CI

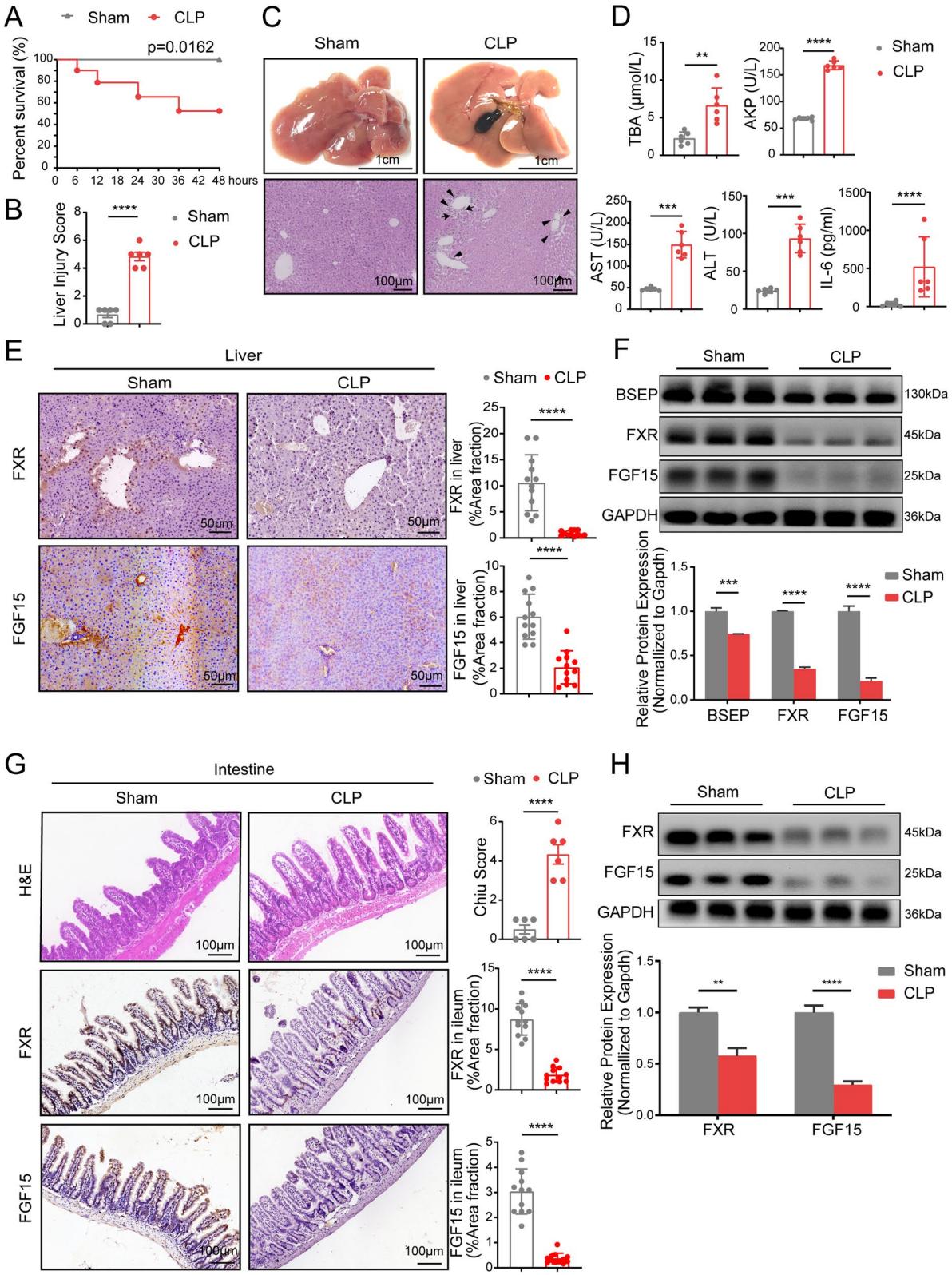

Fig. 1 (See legend on previous page.)

To evaluate the microbiota barrier in intra-abdominal sepsis, we compared the intestinal microbiota composition in Sham and CLP mice. Microbial DNA extracted from cecal samples was utilized to generate amplicons of the V3-V4 hypervariable regions of the bacteria 16S ribosomal RNA (rRNA) gene, which were then sequenced using Illumina MiSeq. Non-metric multidimensional scaling (NMDS) analysis based on Weighted Unifrac distance displayed a clear separation between Sham and CLP mice (stress < 0.05) (Fig. 2E). Venn diagrams indicated that 486 of the 960 operational taxonomic units (OTUs) were shared between the two groups, with 160 and 314 OTUs predominantly detected in CLP and Sham mice, respectively (Fig. 2F). OTUs with the most significant changes (|log2(FC)|> 5) are highlighted in the volcano map (Fig. 2G). A histogram comparison of family-level microbiome diversity revealed a marked reduction in Lactobacillaceae and Lachnospiraceae, while Erysipelotrichaceae, Ruminococcaceae, Desulfovibrionaceae, Bacteroidaceae, and Rikenellaceae were increased in the CLP group compared to the Sham group (Fig. 2H). At the genus-level, Lactobacillus and Bifidobacterium were diminished, whereas Allobaculum, Bacteroides, Oscillospira and Enterococcus were elevated in the CLP group (Fig. 2I). Using the LEfSe method for nonparametric tests and linear discriminant analysis, we identified Lactobacillus as a characteristic genus in the Sham group and Bacteroides in the CLP group (LDA > 4.8) (Fig. 2J). These findings indicate that the intestinal flora of CLP mice was profoundly disrupted, with Lactobacillus being downregulated and Bacteroides upregulated.

In brief, sepsis severely compromises the intestinal barrier, leading to impaired intestinal function and altered microbiota composition.

The treatment with FXR agonist, INT-747, enhanced gut barrier function and conferred protection against intra-abdominal sepsis

Previous studies [32–35] have indicated a substantial decline in FXR expression during sepsis. To further explore the direct impact of FXR on the intestinal barrier, we intervened in mice using a selective FXR agonist, INT-747 (also known as Obeticholic Acid). Mice that underwent CLP surgery and were gavaged with INT-747 30 min later were designated as the CLP + INT group, while control mice gavaged with an equivalent amount of PBS were named the CLP + Vehicle group.

The results revealed that the 7-day survival rate of mice in the CLP + INT group reached 60%, higher than that of the CLP + Vehicle group (30%) (Fig. 3A). INT-747 effectively prevented the shortening of gastrointestinal tract length and the reduction of intestinal contents in CLP mice (Fig. 3B). As anticipated, FXR and FGF15 expression in the ileum of the CLP + Vehicle group was significantly lower than that in the Sham group. However, INT-747 administration increased their levels in mice 24 h after CLP (Fig. 3C). We then compared gut barrier function among the three groups. H&E staining showed that INT-747 treatment in CLP mice resulted in lower Chiu Scores (Fig. 3D), increased goblet cell proliferation (Figure S1 A), an elevated villi/crypt ratio (Figure S1B), and enhaced proliferation of intestinal epithelial cells, compared to the CLP + Vehicle group. Immunofluorescence staining revealed upregulated expression of ZO-1 and Mucin-2 (Fig. 3D), while IHC showed reduced CD45 expression, indicating improved intestinal barrier function in the CLP + INT group compared to the CLP + Vehicle group (Fig. 3D). Western blot analysis confirmed that FXR and FGF15 were directly upregulated by INT-747 (Figure S1 C).

(See figure on next page.)

Fig. 2 Intestinal barrier function was severely compromised in sepsis. **A** Alcian blue staining revealed a reduced number of goblet cells in the ileum of the CLP group. $n = 6$ per group. Scale bars represent 100 μm. **B** Representative of ZO-1 and Mucin-2 immunofluorescence staining and quantitative analysis in Sham and CLP groups. $n = 6$ per group. Scale bars represent 100 μm. **C** Western blot (up) and quantitative analysis (down) of ZO-1 and CD45 protein in ileum from Sham and CLP mice. All measurements were normalized by using GAPDH expression as an internal standard. $n = 3$ per group. **D** Immunohistochemical staining and quantitative analysis for CD45 and CD11b. $n = 6$ per group. Scale bars represent 100 μm. **E** V3-V4 hypervariable regions of the bacteria 16S ribosomal RNA (rRNA) gene extracted from cecal samples were detected by Illumina MiSeq sequencings. Mouse cecal bacterial communities were clustered using Non-metric multidimensional scaling (NMDS) analysis of the UniFrac weighted distance matrix. The stress value is indicated on the graph (stress < 0.05). Each dot represents a cecal community. $n = 6$ per group. **F** Venn diagram of differential amplicon sequence variants in Sham and CLP groups. $n = 6$ per group. **G** Volcanic maps with statistically significant distributions (log p values) and magnitude of change (log2 fold change) of differentially expressed miRNAs in two groups. The right dots represent significantly upregulated genes, while the left dots represent significantly downregulated genes. $n = 6$ per group. **H**-**I** Histogram of microbiome diversity were used to compare the relative abundances of the Sham and CLP groups at the family and genus levels. $n = 6$ per group. **J** Linear discriminant analysis (LDA) effect size (LEfSe) analysis identified the taxa with the greatest differences in abundance at the genus level between the Sham and CLP groups. Only significant taxa meeting a LDA threshold value of > 3.6 are shown here. Each transverse column represents a species, and the length of the column correspond to the LDA value, the higher the LDA value, the greater the difference. $n = 6$ per group. All data were displayed as mean ± SEM and were considered significant at $p < 0.05$ (*), $p < 0.01$ (**), $p < 0.001$ (***), and $p < 0.0001$ (****). Unpaired two-tailed t-tests were used, and the bars represent the mean and 95% CI

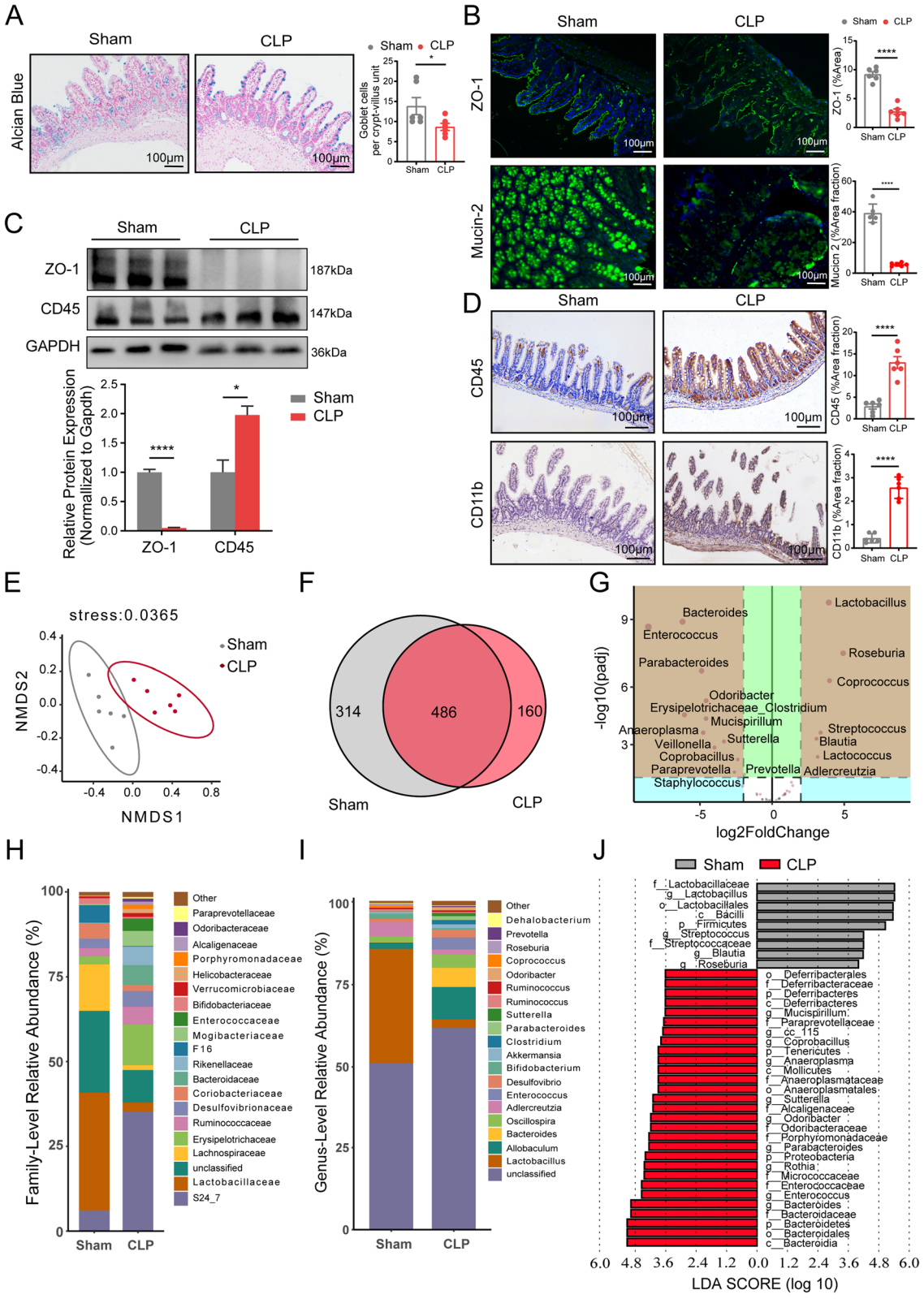

Fig. 2 (See legend on previous page.)

To determine whether INT-747 treatment ameliorates intestinal dysbiosis, we performed 16S rRNA sequencing on fecal samples from the three groups of mice. The results indicated that INT-747 treatment increased the richness of the intestinal microbiota, with 725 OTUs identified in the CLP + INT group, compared to 685 in the CLP + Vehicle group and 818 in the Sham group (Figure S1D). NMDS analysis based on Weighted Unifrac distance showed distinct segregation in microbiota composition among the three groups (stress < 0.1) (Figure S1E). Consistent with the positive correlation between sepsis severity and acute pro-inflammatory cytokines such as IL-6, TNF-α, and IL-1β, redundancy analysis (RDA) also revealed a positive association between sepsis severity and total bile acid (TBA) levels (Figure S1 F). This analysis was primarily used to elucidate the relationship between the bacterial flora and environmental factors and to identify key environmental drivers affecting sample distribution. A detailed analysis of the relative abundance at the phylum and genus levels revealed increased Lactobacillus and decreased Bacteroidetes and Oscillospira in the CLP + INT group compared to the CLP + Vehicle group, indicating a shift towards beneficial and away from detrimental intestinal microbiota (Figure S1G).

In a nutshell, INT-747 treatment enhanced intestinal barrier function and mitigated intestinal injury induced by intra-abdominal sepsis. Direct activation of FXR reversed the progression of sepsis and concurrently increased the abundance of beneficial intestinal microbiota.

Intestinal epithelial cell Myd88-specific deficiency enhances gut barrier function

The expression of intestinal Myd88 was conspicuously augmented in the ileum of septic mice (Fig. 4A). Given that Myd88 and FXR expression show opposite trends during sepsis, we sought to elucidate the role of Myd88 in FXR regulation using $Myd88^{\Delta IEC}$ mice, which is defined as intestinal epithelial Myd88-specific knockout mice, mice with specific deletion of Myd88 in intestinal epithelial cells. CLP and control surgeries were performed on $Myd88^{\Delta IEC}$ mice and their control $Myd88^{fl/fl}$ mice, resulting in four groups: $Myd88^{fl/fl}$-Sham, $Myd88^{\Delta IEC}$-Sham, $Myd88^{fl/fl}$-CLP, and $Myd88^{\Delta IEC}$-CLP mice. We compared the gut barrier function among these four groups.

Histological analysis of intestinal sections revealed significantly higher Chiu scores in both the $Myd88^{fl/fl}$-CLP and $Myd88^{\Delta IEC}$-CLP groups compared to their respective controls. Notably, a significant difference was observed between the two CLP groups (Fig. 4C). These findings are consistent with the established knowledge that sepsis often leads to decreased villus height, increased crypt depth, and slower enterocyte migration [36, 37]. Additionally, both CLP groups showed a decline in the villus/crypt ratio and a decrease in goblet cell number compared to their respective Sham groups, although no significant difference was observed between the two CLP groups (Figure S2A, B). Immunohistochemistry and Western blot analysis of CD45 showed increased leukocyte infiltration in the ileum of both CLP groups, with a more pronounced increase in the $Myd88^{fl/fl}$-CLP group compared to the $Myd88^{\Delta IEC}$-CLP group (Fig. 4B, C). Concurrently, serum levels of IL-6 and IL-1β were significantly reduced in $Myd88^{\Delta IEC}$-CLP mice compared to $Myd88^{fl/fl}$-CLP mice (Figure S2C, D). These results affirm that $Myd88^{\Delta IEC}$-CLP mice exhibit reduced intestinal pathology and a less intense systemic inflammatory response compared to $Myd88^{fl/fl}$-CLP mice.

Furthermore, 24 h after CLP surgery, the expression of ZO-1 was conspicuously diminished and nearly absent in the apical region of the villi in $Myd88^{fl/fl}$-CLP mice. In contrast, ZO-1 expression was significantly higher in the $Myd88^{\Delta IEC}$-CLP group, a finding further confirmed by Western blot analysis (Fig. 4B, C). During intestinal infection, reduced Mucin-2 levels can disrupt the mucus layer, a critical component of mucosal barrier function. In this study, Mucin-2 was nearly undetectable in the $Myd88^{fl/}$

(See figure on next page.)

Fig. 3 INT-747 improved gut barrier function and protected against intra-abdominal sepsis. **A** The 7-day survival rate was compared in the Sham, CLP + Vehicle, and CLP + INT groups. Log-rank (Mantel-Cox) test were used for statistical analysis. $n = 8$ per group. **B** Gross specimens of the gastrointestinal tract in the Sham, CLP + Vehicle and CLP + INT groups. A standard centimeter scale was used. The gastrointestinal tract length in three groups were statistically compared. $n = 8$ per group. **C** Immunohistochemical staining and quantitative analysis of FXR and FGF15 in the ileum were compared among the Sham, CLP + Vehicle, and CLP + INT group of mice. 3 mice in each group with 4 sections in each group were randomly measured. Scale bars represent 50 and 100 μm respectively. **D** The structure and function of the gut barrier were compared among the three groups. H&E staining and Chiu scores, ZO-1 immunofluorescence staining and fluorescence quantitative analysis, Mucin-2 immunofluorescence staining and the thickness of mucus, and ileal CD45 IHC staining and quantitative analysis were presented in three groups respectively. Scale bars represent 100 μm. All data were graphed as mean ± SEM and were considered significant at $p < 0.05$ (*), $p < 0.01$ (**), $p < 0.001$ (***), and $p < 0.0001$ (****). ns means that there was no statistical difference between the two groups. One-way ANOVA was used in three group comparisons, and the bars represent the mean and 95% CI

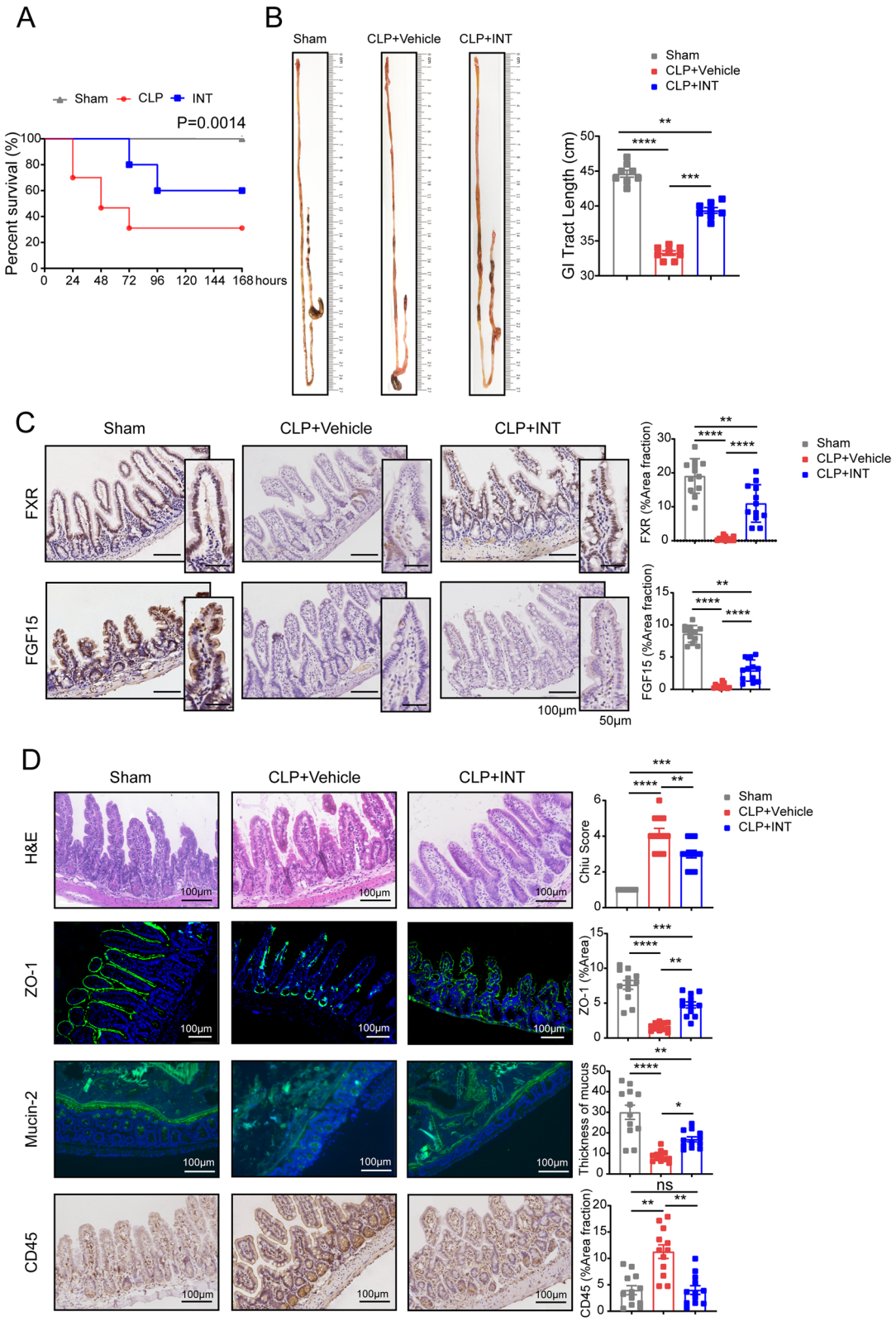

Fig. 3 (See legend on previous page.)

^{fl}-CLP group, while a small but significant increase was observed in the Myd88$^{\Delta IEC}$-CLP group compared to the Myd88$^{fl/fl}$-CLP group (Fig. 4C).

To investigate the relationship between gut microbiota and intestinal permeability, we performed fluorescence in situ hybridization (FISH) combined with 16S rRNA gene sequencing. FISH staining revealed bacterial translocation in Myd88$^{fl/fl}$-CLP mice, which was significantly reduced in Myd88$^{\Delta IEC}$-CLP mice (Fig. 4C). Additionally, we assessed intestinal permeability by administering FITC-dextran via gavage. Myd88$^{\Delta IEC}$-CLP mice exhibited reduced permeability compared to Myd88$^{fl/fl}$-CLP mice (Figure S2E).

In short, compared to Myd88$^{fl/fl}$-CLP mice, Myd88$^{\Delta IEC}$-CLP mice showed less impairment of intestinal barrier function, reduced bacterial translocation, and fewer intestinal and systemic inflammatory alterations 24 h after the onset of sepsis.

Intestinal epithelial cell Myd88-specific deficiency upregulates FXR expression and prevents CLP-induced BAs metabolic disturbance

Survival rates, FXR-FGF15 signaling expression, and BA profiles were compared among Myd88$^{fl/fl}$-CLP and Myd88$^{\Delta IEC}$-CLP mice. Notably, Myd88$^{fl/fl}$-CLP mice had a poor 30-day survival rate of only 10%, while Myd88$^{\Delta IEC}$-CLP mice exhibited a significantly higher survival rate of 40%, highlighting the protective effect of Myd88 knockout in intestinal epithelial cells (Fig. 5A). Both groups experienced similar weight loss 24 h post-surgery (Fig. 5B). Liver injury scores were slightly higher in both CLP groups compared to the Sham group, with no significant differences (Fig. 5C).

Protein expression analysis revealed that Myd88 knockout in intestinal epithelial cells reduced hepatic Myd88 expression, attenuating liver inflammation (Fig. 5C, D). FXR and FGF15 expression were significantly decreased in Myd88$^{fl/fl}$-CLP mice, but were preserved in Myd88$^{\Delta IEC}$-CLP mice (Fig. 5D). This prevented the downregulation of BSEP and the upregulation of CYP7 A1, maintaining BA homeostasis. Consequently, TBA in serum were lower in Myd88$^{\Delta IEC}$-CLP mice compared to Myd88$^{fl/fl}$-CLP mice 24 h after CLP (Fig. 5E).

BA profiles in the liver were further analyzed. CLP induced significant increases in various BAs, including cholic acid (CA), ursodeoxycholic acid (UDCA), taurocholic acid (TCA), taurochenodeoxycholic acid (TCDCA), α-muricholic acid (αMCA), taurocholic α-muricholic acid (TαMCA), β-muricholic acid (βMCA), taurocholic β-muricholic acid (TβMCA), ω-muricholic acid (ωMCA), and taurocholic ω-muricholic acid (TωMCA) 24 h after CLP. These BA disturbances were mitigated in Myd88$^{\Delta IEC}$-CLP mice compared to Myd88$^{fl/fl}$-CLP mice (Fig. 5F). Conversely, levels of deoxycholic acid (DCA) and UDCA were significantly decreased by CLP, but restored in Myd88$^{\Delta IEC}$-CLP mice (Fig. 5F).

Since the composition of BAs can directly influence the gut microbiota, we also analyzed the gut microbiomes in the two CLP groups using 16S rRNA sequencing. Beta diversity analysis showed distinct clustering between Myd88$^{\Delta IEC}$-CLP and Myd88$^{fl/fl}$-CLP mice (stress < 0.1) (Fig. 5G). Alpha diversity indices (Chao1, Observed features, Shannon, and Simpson) revealed that the gut microbiota in Myd88$^{\Delta IEC}$-CLP mice were significantly more diverse than in Myd88$^{fl/fl}$-CLP mice (Fig. 5H, Figure S2F-H).

In Myd88$^{\Delta IEC}$-CLP mice, intestinal inflammation was reduced compared to Myd88$^{fl/fl}$-CLP mice (Fig. 5B). The expression of FXR in ileum was significantly reduced, which was consistent with the situation in the liver. Similarly, the absence of Myd88 in the intestinal epithelium effectively precluded the reduction of FXR (Fig. 5B). These results collectively suggest that intestinal epithelial Myd88 knockout effectively upregulated FXR, reduced intestinal inflammation, and enhanced barrier function in abdominal sepsis.

Collectively, these data demonstrate that intestinal epithelial Myd88 deficiency upregulates FXR-FGF15 signaling and alleviates CLP-induced BA metabolic disturbances.

(See figure on next page.)

Fig. 4 Intestinal epithelial cell Myd88-specific deficiency improves gut barrier function. **A** Compared with Sham group mice, the expression of intestinal Myd88 protein (up and middle) and mRNA (down) were abundantly detected in the intestine 24 h after CLP. All measurements were normalized by using GAPDH expression as an internal standard. $n = 3$ per group. **B** Protein expression and the abundance analysis of FXR, FGF15, Myd88, ZO-1 and CD45 in the ileum were compared among the four groups, namely Myd88$^{fl/fl}$-Sham, Myd88$^{fl/fl}$-CLP, Myd88$^{\Delta IEC}$-Sham, and Myd88$^{\Delta IEC}$-CLP four groups by western blot. All measurements were normalized by using GAPDH expression as an internal standard. $n = 3$ per group. **C** The structure and function of the gut barrier were compared among the four groups. Intestinal H&E staining and Chiu scores, representative CD45 IHC staining and quantitative analysis, ZO-1 immunofluorescence staining and fluorescence quantitative analysis, Mucin-2 immunofluorescence staining and the thickness of mucus were shown. Fluorescence in situ hybridization (FISH) test were implemented among the four groups. The red stain is the bacteria in the intestinal cavity, the blue DAPI stain is the nucleus, and the white arrow indicates leaking bacteria. 3 mice in each group with 4 sections were randomly measured. Scale bars represent 50 μm. All data were displayed as mean ± SEM. An unpaired two-tailed t-test was used between the two groups and a two-way ANOVA with Tukey's multiple comparison test was performed among multiple groups. Bars represent the mean and 95% CI. Considered statistically significant at $p < 0.05$ (*), $p < 0.01$ (**), $p < 0.001$ (***), and $p < 0.0001$ (****). ns means that there was no statistical difference between the two groups. The bars represent the mean and 95% CI

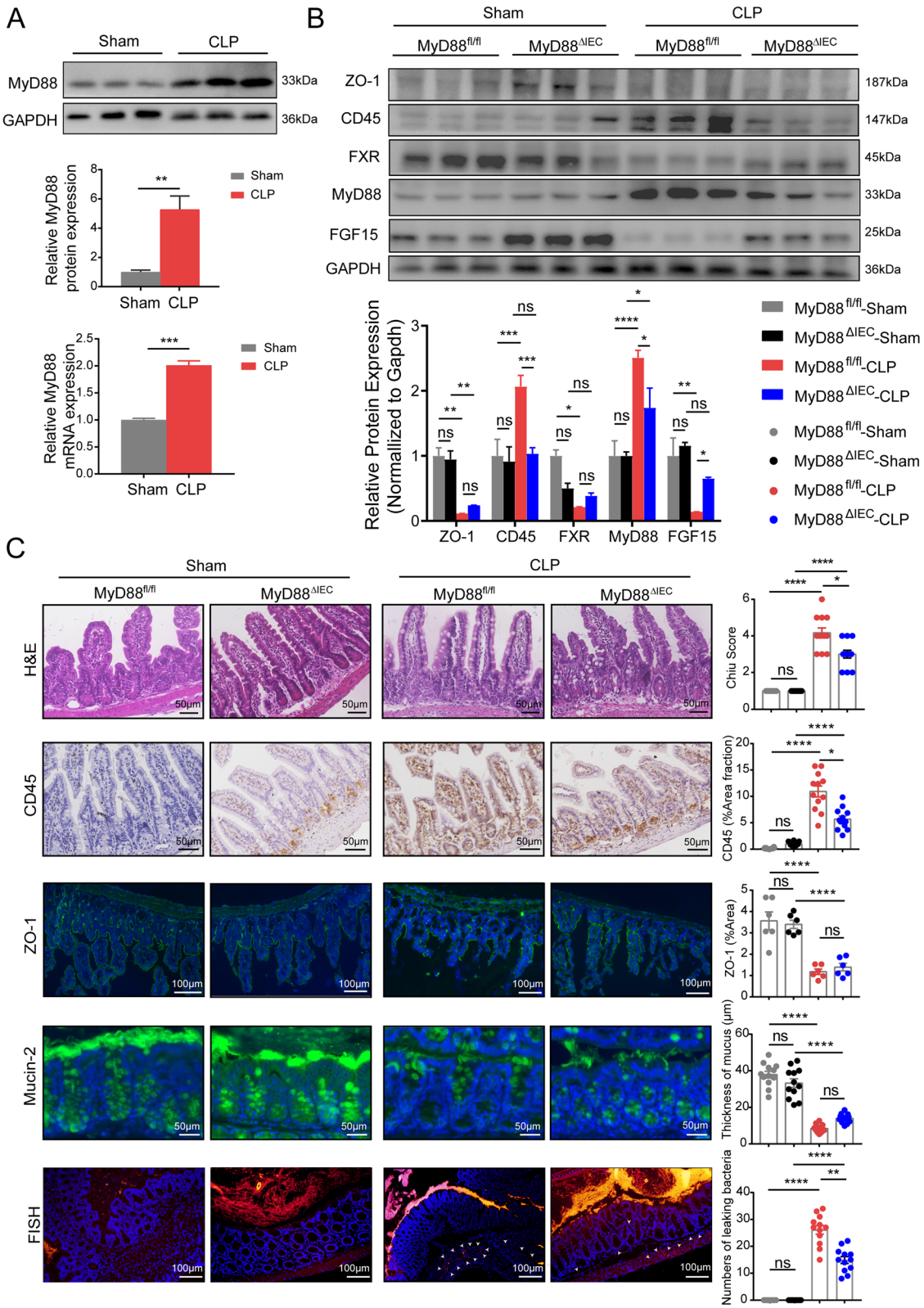

Fig. 4 (See legend on previous page.)

Sepsis-derived microbiota exacerbates the disorder of intestinal microbiota by activating intestinal Myd88

It is widely acknowledged that Myd88 is intimately associated with sepsis and the intestinal microbiota [23–25]. To explore whether septic flora directly affect intestinal epithelial Myd88, we performed fecal microbiota transplantation (FMT) using normal feces from WT-Sham mice and septic feces from WT-CLP mice into WT recipient mice. We then measured Myd88 mRNA expression in the ileum of both groups (Fig. 6A, left). The FMT procedure was conducted over 7 consecutive days following 4 weeks of selective digestive decontamination (SDD). Results showed that sepsis-derived microbiota activated intestinal Myd88 (Fig. 6B).

To further substantiate whether septic flora affect intestinal microbiota, barrier function, and the FXR-FGF15 axis via intestinal Myd88, we performed FMT on $Myd88^{\Delta IEC}$ mice and their control $Myd88^{fl/fl}$ mice. After SDD, FMT was carried out for 7 consecutive days using septic feces from WT-CLP mice (Fig. 6A, right).

The FXR-FGF15 axis and intestinal barrier function were detected in $Myd88^{\Delta IEC}$-FMT and $Myd88^{fl/fl}$-FMT mice. FXR and FGF15 expression was higher in the intestines of $Myd88^{\Delta IEC}$-FMT mice than in $Myd88^{fl/fl}$-FMT mice (Fig. 6C, D), suggesting that Myd88 deficiency protected against the downregulation of the FXR-FGF15 axis induced by dysbiotic microbiota in CLP mice. Both groups exhibited mucosal damage, crypt proliferation, and goblet cells reduction, but the $Myd88^{\Delta IEC}$-FMT group performed slightly better (Fig. 6E). Additionly, ZO-1 loss was more extensive in the $Myd88^{fl/fl}$-FMT group, indicating greater disruption of villus epithelial continuity (Fig. 6E, F). Immunohistochemistry for CD11b and Western blot for CD45 revealed more pronounced inflammatory infiltration in the $Myd88^{fl/fl}$-FMT group compared to the $Myd88^{\Delta IEC}$-FMT group (Fig. 6E, F).

In summary, these results indicate that septic microbiota can exacerbate intestinal dysbiosis, inhibit the FXR-FGF15 axis, and compromise intestinal barrier function by activating intestinal Myd88.

Probiotic intervention improved septic gut flora, inhibited over-activated Myd88, upregulated FXR-FGF15, regulated BAs metabolism and ultimately promoted barrier function

Previous studies have shown that intestinal dysbiosis activates intestinal epithelial Myd88, which affects the FXR-FGF15 axis—a key pathway in BA metabolism. Reduced FXR expression exacerbates intestinal barrier dysfunction. Therefore, we administered probiotics to correct intestinal dysbiosis in sepsis and examined their effects on intestinal epithelial Myd88, FXR, and intestinal barrier function. Mice receiving probiotics were designated as the CLP + Probiotic group, while controls receiving an equal volume of PBS were designated as the CLP + Vehicle group. Probiotic administration methods are detailed in the materials section.

Body weight changes were compared between the CLP + Vehicle and CLP + Probiotic group at 0 h, 1 h, 6 h, 24 h post-CLP. Probiotic treatment reduced weight loss at 24 h (Fig. 7A) and increased the 24-h survival rate compared to the CLP + Vehicle group (Fig. 7B). Probiotic intervention before and after CLP reduced intestinal Myd88 expression and increased FXR and FGF15 expression, as confirmed by qPCR, WB, and IHC (Fig. 7C-E). Additionally, probiotics altered hepatic BA metabolism, decreasing primary BAs (e.g., CA, β-MCA, TCA) and increasing secondary BAs (e.g., DCA, LCA, UDCA) (Fig. 7G).

(See figure on next page.)

Fig. 5 Intestinal epithelial cell Myd88-specific deficiency upregulates FXR expression and prevents CLP-induced BAs metabolic disturbance. **A** The mice in $Myd88^{fl/fl}$-Sham, $Myd88^{fl/fl}$-CLP, $Myd88^{\Delta IEC}$-Sham, and $Myd88^{\Delta IEC}$-CLP groups were observed for survival up to 30-days after CLP modeling. Mantel-Cox log-rank test was used for statistical analysis. $n = 10$ per group. **B** Comparison of body weight loss 24 h after CLP modeling in four groups of mice: $Myd88^{fl/fl}$-Sham, $Myd88^{fl/fl}$-CLP, $Myd88^{\Delta IEC}$-Sham, and $Myd88^{\Delta IEC}$-CLP. $n = 10$ per group. **C** Comparison of H&E staining of liver (up) and the liver injury scores (down) in four groups of mice. $n = 6$ per group. Scale bars represent 100 μm. **D** Protein abundance analysis of Myd88, BSEP, CYP7 A1, FXR, and FGF15 were conducted by western blot in hepar. All measurements were normalized by using GAPDH expression as an internal standard. $n = 3$ per group. **E** The levels of TBA in the serum of mice were detected by ELISA in four groups. $n = 5$ per group. **F** A comparison of the bile acid spectrum of four groups of mice liver samples, including primary and secondary BAs, bound and free BAs. $n = 5$ per group. CA: cholic acid, CDCA: chenodeoxycholic acid, GCA: glycocholic Acid, TCA: taurocholic acid, TCDCA: taurochenodeoxycholic acid, αMCA: α-muricholic acid, TαMCA: taurocholic α-muricholic acid, βMCA: β-muricholic acid, TβMCA: taurocholic β-muricholic acid, ωMCA: ω-muricholic acid, TωMCA: taurocholic ω-muricholic acid, DCA: deoxycholic acid, LCA: lithocholic acid, UDCA: ursodeoxycholic acid. **G** NMDS based on the UniFrac weighted distance matrix to analyze the beta diversity of cecal bacterial communities in $Myd88^{fl/fl}$-CLP and $Myd88^{\Delta IEC}$-CLP group mice. The stress value was indicated on the graph (stress < 0.1). Each dot represented a cecal community. $n = 7$ per group. **H** Alpha-diversity of gut microbiota profiles in $Myd88^{fl/fl}$-CLP and $Myd88^{\Delta IEC}$-CLP groups by Chao1 index. All data were displayed as mean ± SEM. An unpaired two-tailed t-test was used between the two groups and a two-way ANOVA with Tukey's multiple comparison test was performed among multiple groups. Bars represent the mean and 95% CI. Considered statistically significant at $p < 0.05$ (*), $p < 0.01$ (**), $p < 0.001$ (***), and $p < 0.0001$ (****). And ns indicates no statistical difference

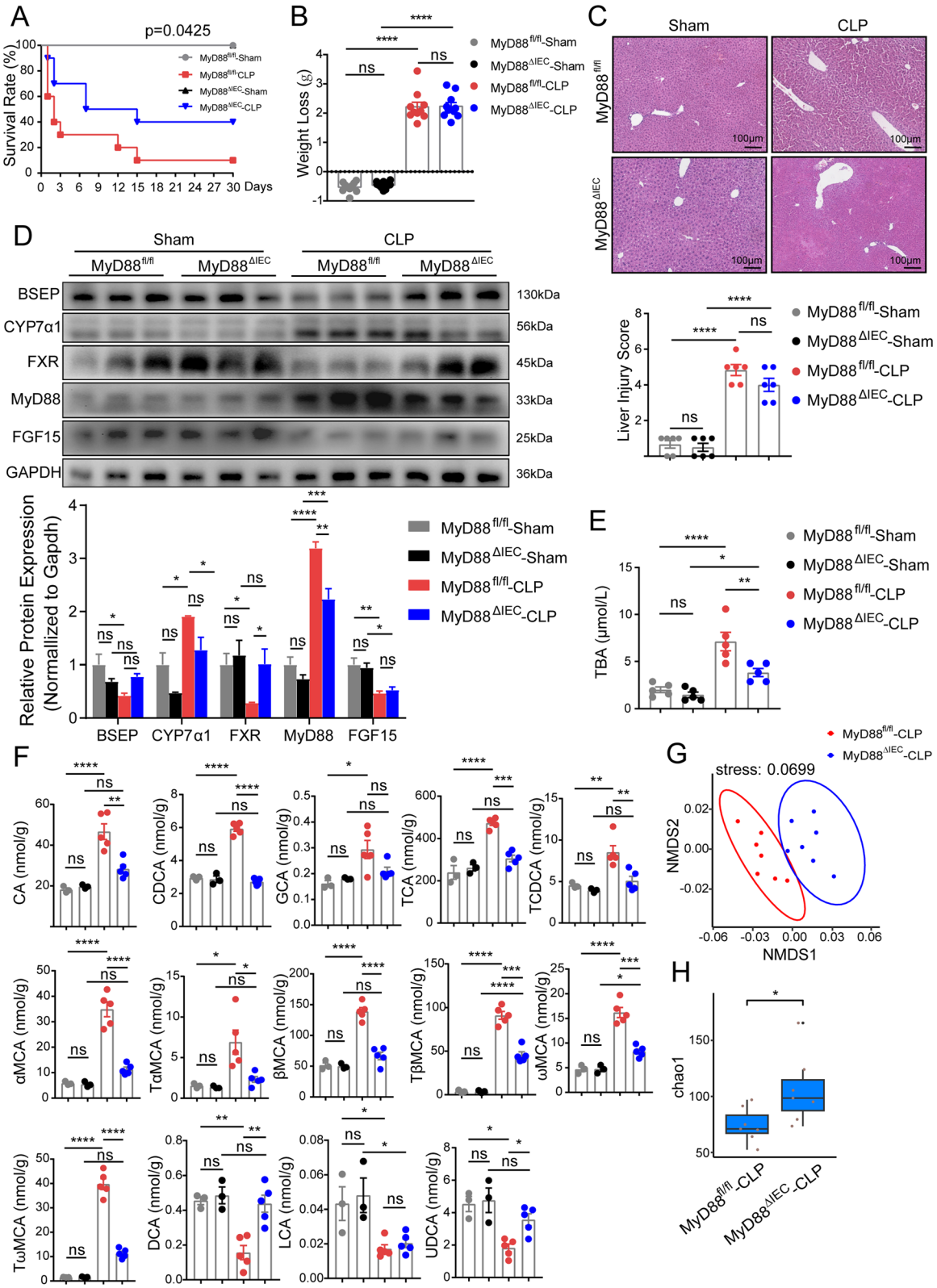

Fig. 5 (See legend on previous page.)

Histologically, H&E staining showed reduced intestinal villus damage in the CLP + Probiotic group, indicated by a lower Chiu score, higher villus-to-crypt (V/C) ratio, and slightly more goblet cells compared to the CLP + Vehicle group (Figure S3 A-B). IHC and Western blot revealed downregulated CD45 and CD11b expression in the CLP + Probiotic group (Figure S3 C, Fig. 7E). Meanwhile, Western blot and immunofluorescence showed upregulated ZO-1 and Mucin-2 expression, indicating improved intestinal barrier function (Fig. 7E, F).

Overall, probiotic supplementation reduced intestinal Myd88 activation, upregulated the FXR-FGF15 axis, improved BA composition, and enhanced intestinal barrier function, ultimately improving mouse survival rates 24 h after CLP.

Discussion

The gut, often referred to as the"motor"of MODS, interacts with other organs such as the lungs, liver, kidneys, and brain, potentially triggering and propagating damage beyond the intestine. Restoring intestinal integrity, enhancing intestinal immunity, and correcting imbalanced gut microbiota represent promising therapeutic approaches for critically ill patients. The interplay between intestinal MyD88 and FXR signaling is a key aspect of this gut-liver crosstalk during sepsis. Our study highlights that MyD88 activation in intestinal epithelial cells is closely associated with suppressed FXR expression and function. This inverse relationship suggests a potential regulatory mechanism where MyD88 activation may directly or indirectly inhibit FXR signaling, thereby exacerbating gut barrier dysfunction and bile acid metabolic disturbances. The time frames selected for our assessments were based on the natural progression of sepsis and the expected timeline for intervention effects. The 24–48 h window post-CLP was chosen to capture the acute phase of sepsis, during which intestinal barrier dysfunction and inflammatory responses are most pronounced. This allowed us to evaluate the immediate efficacy of interventions such as FXR agonists and probiotics in mitigating these acute effects. For interventions with potential longer-term impacts, such as FXR agonist treatment, a 7-day survival assessment was conducted to provide insights into more sustained effects. Similarly, the 30-day survival assessment for $Myd88^{\Delta IEC}$ mice was designed to evaluate the prolonged effects of Myd88 deletion on sepsis outcomes.

The terminal ileum, located at the end of the small intestine and connecting the jejunum to the cecum, is an ideal site for studying intestinal function and pathology due to its stable anatomical structure. It is also a key site for BA metabolism and uptake, with BA receptors like FXR being highly expressed. These receptors modulate signaling pathways within the enterohepatic axis. Additionally, the terminal ileum hosts a rich and diverse microbiota, reflecting the dynamic interactions between gut microbes and the host. Given these characteristics, we focused our investigation on the terminal ileum.

During sepsis, the diversity of the gut microbiota decreases, and the composition of the microbial community changes. Our study found a significant reduction in Lactobacillus and an increase in Bacteroides in sepsis. Lactobacilli can adhere to enterocytes, compete with pathogens for nutrients, secrete antimicrobial substances, lower gut pH, and produce biosurfactants [38, 39]. Reduced Lactobacillus abundance may worsen sepsis outcomes, which could explain the benefits of probiotic treatment. Conversely, Bacteroides is a common

(See figure on next page.)

Fig. 6 Sepsis-derived microbiota exacerbates the disorder of intestinal microbiota by activating intestinal Myd88. **A** Schematic diagram of fecal microbiota transplantation (FMT) experiment. Normal feces from WT-Sham and septic feces from WT-CLP separately transplanting to WT mice to explore the direct effects of septic flora on intestinal epithelial Myd88 (left). To clarify whether the septic flora affects intestinal flora, intestinal barrier function, and the FXR-FGF15 axis via intestinal Myd88, we conducted FMT from WT-CLP mice to intestinal epithelial cell Myd88-specific knockout mice ($Myd88^{\Delta IEC}$) and their control $Myd88^{fl/fl}$ mice (right). After SDD, FMT was carried out for 7 consecutive days. **B** The mRNA expression of Myd88 in ileum was detected in $Myd88^{fl/fl}$-FMT and $Myd88^{\Delta IEC}$-FMT group of mice by qPCR. Gapdh was used as an internal control. Relative mRNA expression was quantified using the comparative CT (ΔCt) method and expressed as $2^{-\Delta\Delta Ct}$. $n = 3$ per group. **C** Immunohistochemical staining and quantitative analysis of ileum Myd88, FXR, and FGF15 were compared in the $Myd88^{fl/fl}$-FMT and $Myd88^{\Delta IEC}$-FMT group. 3 mice with 4 sections in each group were randomly measured. $n = 3$ per group. Scale bars represent 50 μm. **D** Western blot (up) and quantitative analysis (down) of Myd88, FXR, and FGF15 protein in ileum were compared in the $Myd88^{fl/fl}$-FMT and $Myd88^{\Delta IEC}$-FMT group. All measurements were normalized by using GAPDH expression as an internal standard. $n = 3$ per group. **E** The structure and function of the gut barrier were compared between the $Myd88^{fl/fl}$-FMT and $Myd88^{\Delta IEC}$-FMT group. H&E staining and the reduction of goblet cells in each crypt-villus unit, ZO-1 immunofluorescence staining and fluorescence quantitative analysis, and CD11b IHC staining and quantitative analysis were presented in two groups. 3 mice with 4 sections in each group were randomly measured. $n = 3$ per group. Scale bars represent 100 μm. **F** Western blot (up) and quantitative analysis (down) of CD45 and ZO-1 protein in the ileum were compared between the $Myd88^{fl/fl}$-FMT and $Myd88^{\Delta IEC}$-FMT groups. Equal amount of total protein from each sample was loaded and GAPDH was used as loading control. $n = 3$ per group. All data were graphed as mean ± SEM and were considered significant at $p < 0.05$ (*), $p < 0.01$ (**), $p < 0.001$ (***), and $p < 0.0001$ (****). An unpaired two-tailed t-test was used between the two groups. Bars represent the mean and 95% CI

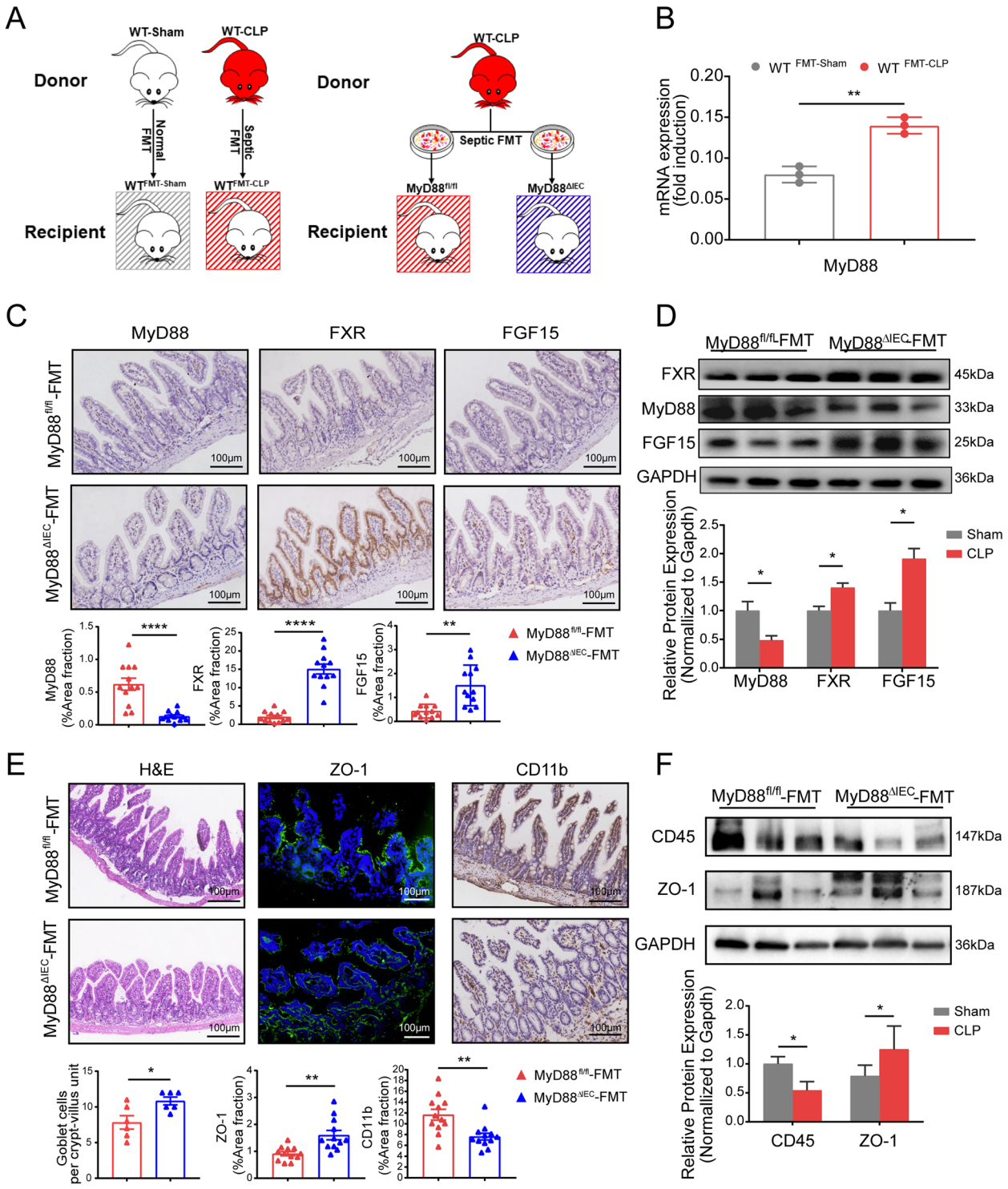

Fig. 6 (See legend on previous page.)

cause of severe sepsis following colorectal surgery [40], and its overgrowth can lead to intra-abdominal infections and bacteremia [41]. Other bacterial families, such as Erysipelotrichaceae, Ruminococcaceae, Desulfovibrionaceae, and Rikenellaceae, were also increased in sepsis models.

In addition to gut flora, sepsis is also associated with a variety of intestinal metabolites, including short-chain

fatty acids (SCFAs), bile acids (BAs), amines, phenols, indoles, vitamins, and others. For instance, in patients with sepsis, the concentrations of SCFAs are significantly reduced. This reduction exacerbates intestinal barrier dysfunction, promotes pathogen colonization, and affects the systemic immune response, with the decreased SCFA levels potentially persisting for up to 6 weeks [42]. Intestinal tryptophan metabolism is also disturbed in sepsis patients, and it is closely related to alterations in the gut microbiota and the severity of sepsis [43]. BAs are another important product of gut microbiota metabolism, playing a role in lipid metabolism and immune regulation. In sepsis, levels of primary bile acids are increased, while levels of secondary bile acids are decreased. This change may affect the metabolic activity of the gut microbiota and, consequently, the intestinal barrier function. BAs can regulate the expression of tight junction proteins (e.g., ZO-1) in intestinal epithelial cells by activating specific receptors (e.g., FXR, TGR5), thereby enhancing the barrier function of intestinal epithelial cells and maintaining the integrity of the intestinal barrier [44]. Additionally, BAs can regulate the thickness of the intestinal mucus layer and promote the proliferation of goblet cells within the mucus layer. This action protects intestinal epithelial cells from pathogens and harmful substances, thereby enhancing the intestinal barrier function [45]. While this study primarily focused on BA dynamics due to their direct relevance to our therapeutic interventions, the broader metabolic network (including polyamines, vitamins, and phenolic compounds) warrants systematic investigation through multi-omics approaches in future studies.

Our study provides evidence that decreased FXR expression contributes to impaired intestinal barrier function during sepsis. Together with other studies [16, 17, 46–48], our research further supports the important role of FXR in gut barrier function. The protective effects of FXR on the intestinal barrier are multifaceted, including direct intestinal benefits, BA metabolism regulation, and microbiota stabilization. Specifically, FXR inhibits pro-inflammatory cytokines, upregulates tight junction proteins, reduces villous cell loss, and thickens the mucus layer, thereby maintaining intestinal barrier integrity [15, 48, 49]. Additionally, the FXR-FGF15 axis is crucial for bile metabolism. Sepsis-associated cholestasis is linked to elevated BA levels and increased mortality [34]. FXR activation in the ileum regulates BA reabsorption via transporters such as ASBT, I-BABP, and OSTα/β [10]. Reduced FXR expression decreases BA reabsorption, while decreased FGF15/19 levels promote BA synthesis via CYP7 A1 upregulation, leading to cholestasis. BA disturbances can further disrupt the gut microbiota and barrier function.

FXR agonists, such as INT-747 (obeticholic acid), show promise in reducing inflammation and improving sepsis-induced cholestasis and intestinal injury. Obeticholic acid upregulates FXR, increases intestinal Lactobacillus, and enhances gut microbiota function, similarly to the previously literature [50, 51]. These effects improve gut barrier function and survival rates in sepsis models. However, randomized controlled trials are needed to confirm the therapeutic potential of FXR agonists in sepsis patients. Despite the clear inverse relationship between MyD88 activation and FXR expression observed in our study, the precise molecular mechanisms underlying this interaction remain to be fully elucidated. Potential pathways, such as NF-κB-mediated transcriptional repression, may

(See figure on next page.)

Fig. 7 Probiotics treatment improved septic gut flora, downregulated Myd88, upregulated FXR-FGF15, and modulated BAs metabolism, ultimately promoted barrier function and survival rate. **A** Body weight changes in CLP + Vehicle and CLP + Probiotic mice at 0 h, 1 h, 6 h, 24 h after CLP. $n = 6$ per group. Two-way ANOVA had been used and Bonferroni statistical hypothesis test was used for multiple comparisons in different times of two groups. There was a statistically significant difference in weight change between the two groups at 24 h ($p = 0.0159$). **B** Survival analysis of CLP + Vehicle and CLP + Probiotic group mice at 24 h after probiotics and PBS administration to CLP mice. Survival rates were not statistically different between the two groups, but were slightly better in the CLP + Probiotic group. Mantel-Cox log-rank test were used for statistical analysis. $n = 6$ per group. **C** The mRNA expressions of intestinal FXR, FGF15, ZO-1, Myd88, CD45 and IL-1β were determined by RT-qPCR, and GAPDH was used to normalize. $n = 3$ per group. **D** Immunohistochemical staining and quantitative analysis of ileal Myd88, FXR, and FGF15 in CLP + Vehicle and CLP + Probiotic group mice were shown. 3 mice with 4 sections in each group were randomly measured. $n = 3$ per group. Scale bars represent 100 μm and 50 μm. **E** Western blot (up) and quantitative (down) of Myd88, FXR, ZO-1, and CD45 protein in ileum from CLP + Vehicle and CLP + Probiotic groups. All measurements were normalized using GAPDH expression as an internal standard. $n = 3$ per group. **F** The structure and function of the gut barrier were compared between the CLP + Vehicle and CLP + Probiotic groups. Intestinal H&E staining and Chiu scores, Mucin-2 and ZO-1 immunofluorescence staining and fluorescence quantitative analysis were shown in two groups. 3 mice in each group with 4 sections were randomly measured. Scale bars represent 50 μm. **G** A comparison of the hepatic bile acid spectrum between the CLP + Vehicle and CLP + Probiotic groups of mice was conducted, and the typical types of bile acids were listed here. $n = 3$ per group. CA: cholic acid, βMCA: β-muricholic acid, TCA: taurocholic acid, DCA: deoxycholic acid, LCA: lithocholic acid, UDCA: ursodeoxycholic acid. All data were graphed as mean ± SEM and were considered significant at $p < 0.05$ (*), $p < 0.01$ (**), $p < 0.001$ (***), and $p < 0.0001$ (****). And ns indicates no statistical difference. An unpaired two-tailed t-test was used between the two groups. Bars represent the mean and 95% CI

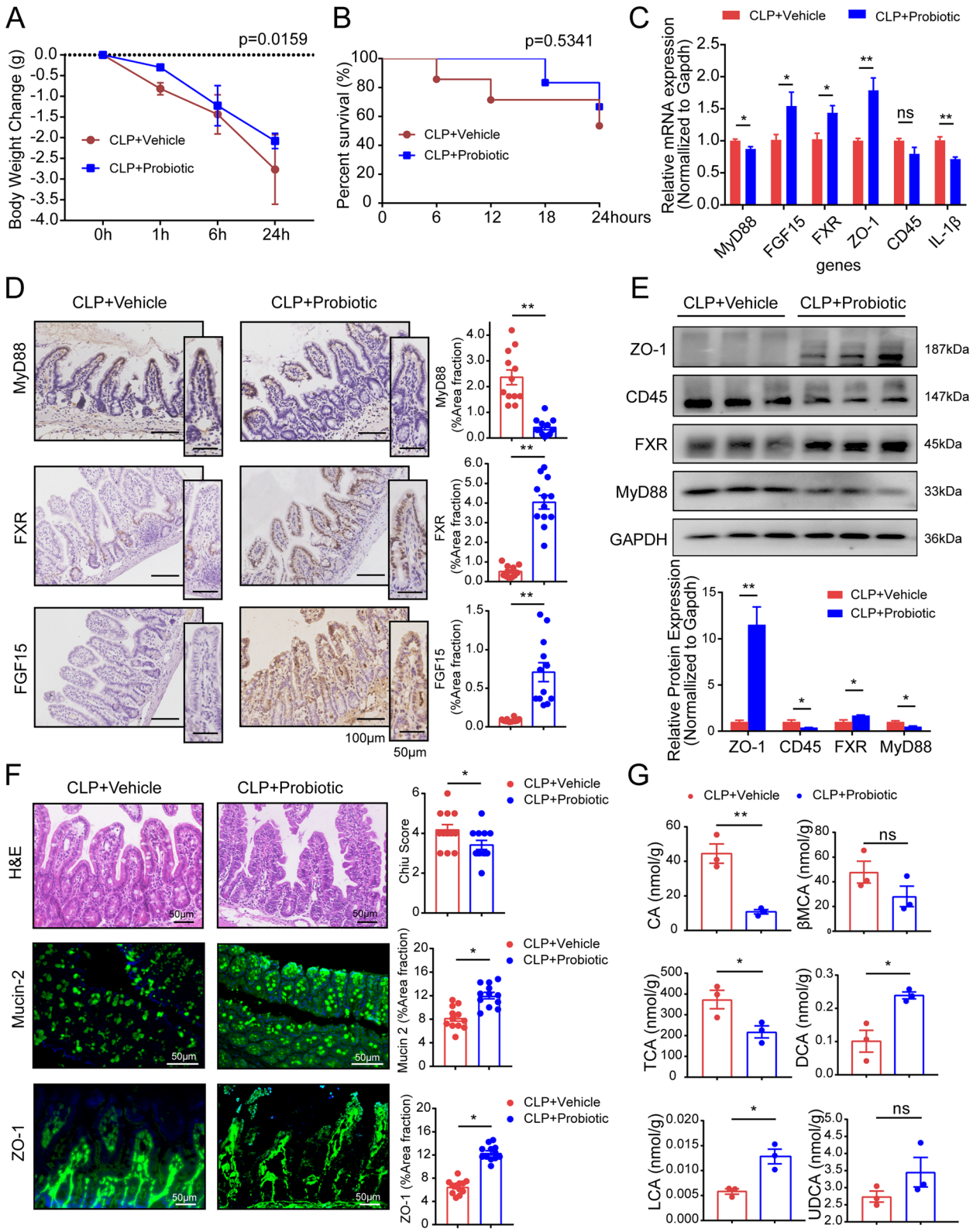

Fig. 7 (See legend on previous page.)

play a role in this process. MyD88, as a central adaptor in TLR signaling, activates NF-κB upon ligand binding [52]. NF-κB, in turn, can regulate the transcription of various genes [53]. It is plausible that activated MyD88 triggers NF-κB signaling, which may directly or indirectly repress FXR transcription. This could occur through competition for transcriptional coactivators or via epigenetic modifications that alter FXR gene expression. Further studies are required to validate these potential mechanisms.

In sepsis, primary BAs (e.g., CA and MCA) accumulate, while secondary BAs (e.g., DCA and LCA) decrease due to impaired microbial metabolism [50]. This imbalance is mitigated in Myd88-deficient mice, suggesting that intestinal Myd88 activation contributes to BA disturbances and microbiota dysbiosis. Our findings indicate that inhibiting intestinal Myd88 can restore FXR-FGF15 expression, improve BA profiles, and enhance intestinal barrier function.

Moreover, we found that downregulation of intestinal FXR expression is a hallmark of sepsis, which can be reversed in Myd88-specific knockout mice derived from intestinal epithelial cells. This reversal leads to enhanced survival rates and intestinal phenotypic recovery. Selective inhibition of intestinal Myd88 elevates FXR-FGF15 expression, thereby enhancing intestinal barrier function. This is supported by upregulation of tight junction protein ZO-1, improved barrier junctions, reduced CD45 expression, and attenuated acute inflammatory responses within the intestinal tract. Additionally, FXR upregulation following Myd88 knockdown in intestinal epithelial cells ameliorates cholestasis and alters BA composition and ratios.

Our study demonstrates that septic flora induces Myd88 expression in intestinal epithelial cells. This upregulation inhibits ileal FXR and FGF15 and impairs the intestinal barrier. The mechanism of this study is supported by the knockout of the MyD88 gene in the intestinal epithelium and evidence related to FMT experiments. In FMT experiments, septic flora increased ileal Myd88 expression, downregulated FXR and FGF15, and breached the barrier in $Myd88^{fl/fl}$-FMT mice. However, these effects were mitigated in $Myd88^{\Delta IEC}$-FMT mice. Sepsis-induced microbiota dysbiosis results in a structural imbalance of the flora and the conversion of conditionally pathogenic bacteria into pathogenic ones, which can activate Myd88 via the TLR-Myd88 pathway [6]. Our findings align with previous studies [24, 54, 55]. Of course, it is not excluded that other sepsis-related factors may also contribute to cholestasis and barrier damage.

Our team's previous research showed that microbiota-mediated reduction in FXR activity impacts the FGF15/FXR/CYP7 A1 axis in cholestatic liver disease [56]. However, the influence of intestinal flora on FXR during sepsis was unclear. Our current study revealed diminished intestinal FXR expression in CLP mice, $Myd88^{fl/fl}$-FMT mice, and CLP + Vehicle mice. Probiotic administration improved post-sepsis dysbiosis and augmented FXR and FGF15 expression, confirming the regulatory role of gut microbiota on intestinal FXR function and its potential to exacerbate biliary stasis.

Patients in the early stages of sepsis exhibited reduced alpha diversity, distinct microbial clusters, and altered gut microbiota structure. Probiotics effectively enhance gut microbiome composition and function in these patients, consistent with findings by Stadlbauer et al. [57]. A growing body of evidence highlights the significant correlation between the gut microbiome and sepsis-related mortality, underscoring the potential of microbiome manipulation as a therapeutic strategy [19]. For example, probiotics and synbiotics can preserve microbiota and gut integrity, helping maintain homeostasis in ICU patients and preventing complications [58]. Data from Ludmila Khailova showed that probiotic, mainly Lactobacillus rhamnosus GG (LGG) and Bifidobacterium longum (BL), improved survival in pediatric experimental sepsis when administered at sepsis onset [59]. Furthermore, synbiotics containing Bifidobacterium and Lactobacillus reduced the incidence of enteritis and ventilator-associated pneumonia in sepsis patients [60]. Research indicates that probiotics enhance intestinal barrier function through multiple mechanisms. They competitively inhibit pathogenic bacteria colonization, upregulate tight junction proteins in intestinal epithelial cells, modulate immune responses to lower inflammatory cytokines, and restore gut microbiota balance. These actions reduce septic mice mortality [59, 61]. Multi-strain probiotic therapy not only lowers sepsis patients'inflammatory markers and improves intestinal function [59, 62, 63], but also creates a "synergistic effect", boosting strains' viability for more stable and effective results [64]. In our study, multi-strain probiotics were given 1 h preoperatively and at 6 and 12 h postoperatively, matching typical clinical sepsis intervention windows. CLP-induced septic mice have a 24-h survival rate of only 50%–70% [65]. To assess broad-spectrum probiotics' immediate survival benefits, we administered them within the first 12 post-surgical hours. However, this approach meant we couldn't evaluate long-term survival over seven days. Our data revealed reduced intestinal Myd88 expression, increased FXR and FGF15 expression, and improved intestinal barrier function, indicating that probiotics enhance intestinal barrier integrity via the Myd88-FXR-FGF15 pathway. This offers a novel perspective on using

probiotics to manage sepsis by bolstering gut health and mitigating inflammation. The ability of probiotics to modulate intestinal MyD88 and FXR expression underscores the therapeutic potential of probiotics in sepsis. However, the specific pathways through which probiotics exert their effects on MyD88 and FXR require further investigation. Future studies could explore whether probiotics directly interact with intestinal epithelial cells to influence MyD88 signaling or whether they act indirectly through modifying the gut microbiota composition and metabolite production. Additionally, in vitro experiments, such as treating enterocyte cultures with TLR ligands, could provide valuable insights into the mechanistic link between MyD88 activation and FXR suppression. These experiments would help clarify whether the observed effects are directly mediated by MyD88-FXR interactions or involve additional regulatory factors. We acknowledge that long-term survival data for probiotic intervention are unavailable in this study. The survival assessment for probiotics was limited to 24 h due to the high mortality rate of CLP-induced septic mice within this critical window. Conducting long-term survival studies with probiotics would require additional resources and experimental design considerations, such as repeated administrations and larger sample sizes. However, we recognize the importance of such data for a comprehensive understanding of the therapeutic potential of probiotics in sepsis and suggest this as a direction for future research.

The correlative evidence from our genetic and FMT experiments suggests a potential mechanism by which microbiota dysbiosis may exacerbate intestinal barrier damage in sepsis. This involves a series of events, including modifications in gut microbiota abundance and composition, activation of intestinal epithelial MyD88 by septic flora, suppression of the FXR-FGF15 axis by activated MyD88, disturbances in BA structure that promote further dysbiosis, and persistent disruption of intestinal barrier function via a detrimental cycle involving the BA enterohepatic axis. While these findings highlight a plausible pathway, it is important to consider that other sepsis-related factors not examined in this study may also contribute to cholestasis and barrier damage.

Putting it all together, sepsis-induced intestinal dysbiosis activates intestinal epithelial Myd88, inhibits the FXR-FGF15 axis, and exacerbates intestinal barrier dysfunction. As a classical mouse model of sepsis, CLP is usually considered to be able to replicate the pathogenesis of human sepsis. Even so, however, (1) immunometabolic differences between rodents and humans may affect the translation of therapeutic responses, (2) the heterogeneity of clinical sepsis etiology far exceeds that of standardized animal models, and (3) the temporal dynamics of the human disease process are difficult to fully simulate. Using a mouse CLP model, our study demonstrates that therapeutic approaches that improve gut microbiota, inhibit intestinal Myd88, or directly upregulate FXR may enhance intestinal barrier integrity and improve survival in sepsis. It is expected to provide some reference value for the mechanism of intestinal barrier damage in human sepsis. However, potential therapeutic strategies still need to be validated through multispecies validation and preclinical optimization.

Conclusion

This study provides evidence that CLP-induced intestinal dysbiosis is associated with activation of MyD88 in intestinal epithelial cells, which correlates with disrupted intestinal barrier function via inhibition of FXR-FGF15 signaling and alterations in bile acid metabolism, including cholestasis. While our genetic and FMT experiments support a mechanistic link between these factors, it is important to note that other sepsis-related factors may also contribute to the observed effects on bile acid metabolism and barrier function. Further research is needed to fully elucidate the complex interplay of factors in sepsis pathogenesis. Treatments such as probiotics, FXR agonists, or specific deletion of intestinal epithelial MyD88 show potential for mitigating the progression of intra-abdominal sepsis.

Outlook

Certain issues warrant further attention within this research. Notably, the intracellular mechanisms underpinning the intestinal barrier protection conferred by the upregulation of the FXR-FGF15 axis—potentially mediated by specific intestinal microbiota or their metabolic products—require elucidation. Additionally, the capacity of the microbiota to modulate the FXR-FGF15 enterohepatic axis necessitates comprehensive investigation. Furthermore, a rigorously controlled RCT to evaluate the improved prognosis in patients with sepsis following obeticholic acid treatment needs to be conducted. Extensive research is essential to delve into and corroborate these findings.

Materials and methods

Animals

$Myd88^{tm1Defr/J}$ (Strain No: 008888) and Tg (Vil1-Cre) 1000Gum/J (Strain No:021504) mice of 8 weeks of age were purchased from Jackson Laboratory (Bar Harbor, ME). To study the role of Myd88 on the gut barrier and FXR-FGF15 axis, as well as the crosstalk between intestinal flora on Myd88 and FXR-FGF15, we generated intestinal epithelial cells Myd88-specific knockout mice, $Myd88^{\Delta IEC}$. For this purpose, $Myd88^{flox/flox}$

mice carrying loxP sites flanking exon 3 of the Myd88 gene were crossed to Vil1-Cre transgenic mice. We first crossed Vil1-Cre$^{+/-}$ mice with Myd88$^{flox/flox}$ mice to generate Myd88$^{flox/+}$/Vil1-Cre$^{+/-}$ animals and then crossed these with Myd88$^{flox/flox}$ mice once again to obtain Myd88$^{flox/flox}$/Vil1-Cre$^{+/-}$ mice (abbreviated as Myd88$^{\Delta IEC}$). Myd88$^{\Delta IEC}$ mice were assigned to the experimental group and Myd88$^{flox/flox}$/Vil1-Cre$^{-/-}$ (abbreviated as Myd88$^{fl/fl}$) mice were as control (C57BL/6 background).

All mice were genetically phenotyped at 4 weeks and housed in the same specific pathogen-free room in individually ventilated cages with free access to a standard chow diet and water. The gene types and the number of mice used in the experimental and control groups are listed in the corresponding legends in each figure. Mice of the same genotype were grouped according to ear labels using random number table method. The person responsible for feeding and the statistician grouped the mice randomly. The experimenter was not aware of the grouping of the mice. The person who stained the sections and analyzed the images was also ignorant of the grouping of the mice from which the samples were taken. Two separate personnel collaborated on each phase of the experiment.

Experimental models

Caecal ligation puncture (CLP) surgical procedure

Polymicrobial sepsis induced by CLP is the most frequently used model to study the pathophysiology of sepsis because it closely resembles the progression and characteristics of human sepsis [66]. CLP procedure is as follows: (i) Mice aged 10–12 weeks were anesthetized with mixture of ketamine and xylazine intraperitoneally, then shaved and disinfected. (ii) Lower abdomen skin was incised midline, then the cecum was isolated and exteriorized, and 75% percent of the distal end of the cecum (about 1 cm) was ligated. (iii) Next, the cecum was p unctured by a 22G needle. The perforation of the cecum consisted by a single through-and-through puncture midway between the ligation and the tip of the cecum in a mesenteric-to-antimesenteric direction. (iv) The cecum was then gently compressed to extrude a small amount of cecal content and returned to the abdominal cavity. (v) The abdominal musculature and the abdominal skin were closed by 3–0 silk sutures respectively. (vi) Fluid resuscitation was given by prewarmed normal saline (37 °C, 50 ml/kg ip.). (vii) Mice were placed on a warm blanket for recovery for about 1 h and then returned to the cage [29]. Sham group mice received the same procedure except that the cecum was not ligated or perforated. The surgical modeling of each mouse was implemented by the same person and controlled within 10 min. All samples were collected at 24 h after CLP, except for the mice used to observe survival. We assessed survival and gut barrier function at 24–48 h post-CLP to capture the acute physiological and pathological changes during sepsis onset, as this period is critical for observing the immediate effects of sepsis and the efficacy of interventions.

Selective digestive decontamination (SDD) and fecal microbiota transplantation (FMT)

Donor mice, which were 10–12 weeks old C57BL/6 wild-type males, provided fresh feces samples 24 h post-CLP. Each mouse contributed approximately 5–6 pieces of feces, which were then mixed with phosphate-buffered saline (PBS) in a 1:3 ratio, thoroughly stirred, and allowed to stand for 30 min. The resulting supernatant was refrigerated at 4 °C and administered by gavage within 2 h at a dosage of 100 µl per mouse.

For the recipient mice, Myd88$^{fl/fl}$ and Myd88$^{\Delta IEC}$ mice began SDD treatment at 6 weeks of age, followed by FMT at 10 weeks. A solution containing four antibiotics, metronidazole (1 g/L), vancomycin (1 g/L), ampicillin (1 g/L), and gentamycin (160 mg/L), was prepared in a 5% sucrose-water solution to replace the drinking water. One month after the initiation of this regimen, the mice received daily fecal bacterial gavage for a week, followed by the collection of tissue samples.

Throughout the FMT experimental period, daily CLP surgery was conducted on five wild-type mice to ensure the recipients received a consistent supply of fresh fecal microbiota.

Probiotics treatment

The probiotics utilized in this study were sourced from Zhongke Yikang Biological Technology Company (Beijing), and each gram contained an aggregate of 11 billion colony forming units (CFU), composed of the subsequent 15 bacterial strains: B. animalis ssp. lactis HNO19, B. animalis ssp. lactis BB-12, B. animalis ssp. lactis Bi07, B. animalis B94, B. bifidum Bb06, B longum R175, L. rhamnosus GG, L. rhamnosus R11, L. casei Lc11, L. helveticus R52, L. paracasei Lpc37, L. plantarum R1012, L. reuteri HA188, L. acidophilus NCFM, S. thermophilus St21. (Abbr: Bifidobacterium =B, Lactobacillus =L, Streptococcus =S). The cryopreserved active probiotic powder was dissolved in PBS at 4 °C, and the solution was administered immediately via gavage. The experimental mice were treated with a probiotic dose of 2*10^9 CFU/0.1 ml by gavage 1 day before, 1 h after, and 12 h after CLP. Mice that received PBS alone were employed as controls. To guarantee the efficacy of the active probiotics, these were freshly prepared. Intestinal tissue samples were collected at 24 h post-treatment.

INT-747 intervention

Obeticholic Acid, an effective selective FXR stimulant, also called INT-747 (Selleck, S7660), was diluted to 1 mg/ml and administered by gavage at 10 μg/g 30 min after CLP. The Sham group merely underwent the same switch-belly operation as CLP. Mice subjected CLP surgery and gavaged with PBS or INT-747 after 30 min were designated as the CLP + Vehicle group or CLP + INT group. The three groups of mice were divided into 2 parts, with 16 mice in each group, of which 8 were used for survival observation and the other 8 collected samples at 24 h after CLP for testing intestinal barrier function. The 7-day survival assessment for FXR agonist treatment and the 30-day survival assessment for $Myd88^{\Delta IEC}$ mice were chosen to evaluate the sustained effects of these interventions on survival outcomes, considering the timeline of their potential biological impacts.

Hematoxylin and eosin staining

The ileum and liver were collected, rinsed in phosphate-buffered saline (PBS), and fixed in 4% neutral-buffered paraformaldehyde for 48 h at 4 °C. Afterwards, the tissues were embedded in paraffin and processed for H&E staining. Tissues were sliced into 3 μm slices, and the sliced tissues were dewaxed, rehydrated in 100% alcohol (II), 100% alcohol (I), 90% alcohol, 80% alcohol, 70% alcohol, and 50% alcohol sequentially, washed with ddH_2O for 2 min. Thereafter, stained with hematoxylin for 2 min, differentiated with hydrochloric acid alcohol for a few seconds, washed for 5 min to return to blue, and then stained with eosin for 2 min. Finally, after dehydration, transparency, and sealing with neutral resin, the tissue pathology was observed and photographed under a microscope.

Alcian blue stain

Sections were dewaxed and rehydrated, and circles were drawn using the immunohistochemical pen. The tissues on the sections were soaked by adding Alcain's acidifying solution for 3 min, then stained by adding Alcain's staining solution for 30 min, rinsed with PBS solution, restained by adding nuclear solid red staining solution for 5 min, rinsed again by PBS for 1 min. The sections were dehydrated in an alcohol gradient, transparent in xylene, and sealed in neutral resin.

Immunohistochemistry

The ileum was fixed in 4% paraformaldehyde for 48 h, embedded in paraffin, and sliced into 3 μm sections. Subsequently, the sections were baked, dewaxed, rehydrated, subjected to antigen retrieved, and the endogenous peroxidase was inactivated by 3% H_2O_2. They were blocked by 5% BSA and incubated overnight by the primary antibody respectively. On the next day, after the second antibody incubation, horseradish peroxidase was used for staining. Primary antibodies included human anti-FXR (1:500, Perseus Proteomics, PP-A9033 A-00), mouse anti-Myd88 (1:500, Santa Cruz Biotechnology, sc-74532), mouse anti-FGF15 (1:500, Santa Cruz Biotechnology, sc-398338), Rb anti-CD45 (1:500, Abcam, ab-10558), Rb anti-CD11b (1:1000, Abcam, ab-133357). The staining positive particles in the intestinal villus were quantitatively analyzed by ImageJ software in randomly 12 high-power fields (× 400, 3 mice in each group and 4 pictures of each mouse).

Western blotting

The ileum and liver were grounded by a cryogenic grinder, and proteins were extracted using a RIPA lysis buffer containing a protease inhibitor, a phosphatase inhibitor, and PMSF (Beyotime, Shanghai, China). Protein concentrations were estimated with a bicinchoninic acid (BCA) protein assay kit (EpiZyme, Shanghai, China) and diluted to the same concentration. After adding the loading buffer, the samples were boiled at 100 °C for 5 min. Then, whole-cell lysates were clarified via centrifugation at 4 °C to remove the insoluble deposit, run on 10% polyacrylamide gels, transferred to nitrocellulose membranes (0.2 μm, GE Whatman, Maidstone, UK), and the membranes were blocked for 1 h in TBST containing 5% non-fat milk and then incubated at 4 °C overnight with the corresponding antibody, respectively. The next day, after washing with TBST 3 times, the blots were incubated with HRP-conjugated secondary antibodies for 1 h at room temperature. After washing with TBST three times again, the immunoreactive bands were visualized using enhanced chemiluminescence substrate (ECL, Thermo Scientific, USA). Finally, the protein bands were detected by ChemiDoc Touch Imaging System (Bio-Rad, Hercules, USA). Antibodies were listed as follows: mouse anti-FXR antibody (1:1000, Biotechne), mouse anti-Myd88 (1:200, Santa Cruz Biotechnology, sc-74532), mouse anti-FGF15 (1:200, Santa Cruz Biotechnology, sc-398338), rabbit anti-BSEP antibody(1:1000,abcam), mouse anti-CYP7α1 antibody (1:100, Santa Cruz), rabbit-anti ZO-1 (1:500, Abcam, ab96587), rabbit-anti CD45 (1:1000, Abcam, ab10558), mouse anti-GAPDH (1:3000, sigma/Merck, G8795), rabbit anti-GAPDH antibody (1:2000, Proteintech), goat anti-rabbit, goat anti-mouse, and rabbit anti-goat HRP-conjugated second antibodies (1:3000, Merck, A0545, A4416, and A8919, Merck, Germany). Immunoblot quantitative analysis was conducted by analyzing the relative protein densitometry with ImageJ software. For all western blots, GAPDH probing was performed as internal control.

Enzyme-linked immunosorbent assay (ELISA)

Serum inflammatory factors such as IL-6, IL-1β, AST, ALT, AKP, and TBA were measured by mouse-specific ELISA kits (NJJC Bio, Nanjing, China & PC-biotech, Shanghai, China) in accordance with the manufacturer's instructions. The results were normalized by protein content and cell number. All assays were performed in duplicate by different researchers, and each experiment was carried out three times.

ZO-1 immunofluorescence

For the in vivo study, the murine was deeply anesthetized with isoflurane. Intestine samples were removed, frozen embedded by OCT (SAKURA 4583, USA), and stored at −80 °C. The intestinal samples were cut into 5 μm frozen sections in a cryostat. The frozen sections were dried, fixed in 4% PFA, washed with PBS (including 0.1% Triton X-100), and blocked with 10% fetal bovine serum respectively. Subsequently, the sections were incubated overnight at 4 °C with rabbit-anti ZO-1 (1:500, Abcam, ab96587). Then, the sections were incubated for 1 h at room temperature with Alexa Fluor 488 conjugated goat anti-rabbit IgG (1:500, Beyotime A0423, China), plus with DAPI (Sigma Aldrich, USA) to stain the cell nuclei. The stained sections were observed by fluorescence microscope (Olympus, Tokyo, Japan). Fluorescence quantitative analysis was performed by two different individuals using ImageJ software.

Mucin-2 immunofluorescence

The ileum tissue containing feces was thoroughly removed and soaked in the Metheca solution (60% Methanol: 30% Chloroform: 10% Glacial acetic acid) for 48 h. Subsequently, it was embedded in paraffin, and cut into 3 μm slices. Then the slices were dewaxed, rehydrated, repaired in the microwave oven, cleaned with PBS, blocked with 5% BSA, and incubated with Mucin-2 (1:1000, Santa Cruz, sc-15334) overnight. On the next day, PBS was used for cleaning again, and the slices were stained with a fluorescent secondary antibody (1:500, Beyotime A0423, China) for 1 h. After another PBS cleaning, DAPI was used for sealing, and the slices were photographed with a fluorescent microscope.

Intestinal permeability measurement

The intestinal barrier permeability was evaluated by 4 kDa fluorescein isothiocyanate-conjugated (FITC) dextran after CLP 24 h. As the FITC dextran measured in plasma 1 h after its oral application is a marker of small intestinal permeability. Briefly, overnight fasted mice were orally administered with 25 mg/mL of 4 kDa FITC-Dextran (0.5 mg/g; Sigma-Aldrich). Plasma was collected after 1.5 h, and the fluorescence concentration was measured at excitation and emission wavelengths of 485 nm and 535 nm, respectively.

High throughput sequencing of 16S rRNA

Microbial DNA was extracted from fecal samples by employing the Mag-Bind Soil DNA Kit (Omega Bio-Tek, USA) in accordance with the manufacturer's protocols. The final DNA concentration and purification were ascertained using NanoDrop 2000 UV–vis spectrophotometer (Thermo Scientific, Wilmington, USA), and the DNA quality was inspected by 1% agarose gel electrophoresis. The V3-V4 hypervariable regions of the bacteria 16S rRNA gene were amplified with primers 338 F (5'-ACTCCTACGGGAGGCAGCAG-3') and 806R (5'-GGACTACHVGGGTWTCTAAT-3') through the thermocycler PCR system (GeneAmp 9700, ABI, USA). The PCR reactions were conducted using the following program: 3 min of denaturation at 95 °C, 30 cycles of 30 s at 95 °C, the 30 s for annealing at 55 °C, and 45 s for elongation at 72 °C, and a final extension at 72 °C for 10 min. PCR reactions were executed in triplicates 20 μl mixture containing 4 μl of 5× FastPfu Buffer, 2 μl of 2.5 mM dNTPs, 0.8 μl of each primer (5 μM), 0.4 μl of FastPfu Polymerase and 10 ng of template DNA. The resultant PCR products were extracted from a 2% agarose gel and further purified using the AxyPrep DNA Gel Extraction Kit (Axygen Biosciences, Union City, CA, USA) and quantified by means of QuantiFluor™-ST (Promega, Wisconsin, USA) according to the manufacturer's protocol. All data about 16 s rRNA sequences, analysed in our study, have been deposited in the Sequence Read Archive (SRA) under the accession number: PRJNA1043046, PRJNA1167785, PRJNA1043466. The 16S rRNA sequence data generated in our study have been deposited in the Sequence Read Archive (SRA) under the accession numbers PRJNA1043046, PRJNA1167785, and PRJNA1043466.

Microbiota analysis

Total DNA was extracted from the fecal samples of mice. Hypervariable V3-V4 regions of the bacterial 16S rRNA gene were amplified by PCR specific with 338 F-806R primers, and the PCR products were sequenced by the NovaSeq platform (Illumina, San Diego, USA). Feature sequence also named OTU (Operational Taxonomic Units) were quality-filtered, denoised, merged and non-chimeric using the DADA2 plugin of QIIME 2 software. The abundance and diversity index were analyzed based on OTUs, and cluster analysis and statistical comparison were conducted based on the composition of species in different groups to identify significantly related flora. Alpha diversity was used to describe the microbial

richness. Indices such as observed features, Chao1 richness estimator, Shannon entropy and Simpson index were calculated to estimate the microbial diversity within an individual sample. Beta diversity was performed to investigate the structural variation of microbial communities. The distances of Bray Curtis, unweighted UniFrac, and weighted UniFrac were calculated and analyzed by principal coordinate analysis (PCoA) and non-metric multidimensional scaling (NMDS). Redundancy analysis (RDA) analysis, also known as multivariate direct gradient analysis, is a combination of correspondence analysis and multiple regression analysis, and each step of calculation is regression with environmental factors. RDA was conducted to reveal the association of microbial communities with environmental factors based on relative abundances of microbial species at different taxa levels.

Quantitative real-time PCR

To determine relative gene expression in the ileum, RNA was isolated by using TRIZOL (Invitrogen, Carlsbard, CA, USA) following the manufacturer's instructions, and quantified by a NanoDrop1000 spectrophotometer (Thermo Fisher Scientific, Waltham, MA, USA). cDNA was processed with the cDNA synthesis kit (Thermo Fisher Scientific, Waltham, MA, USA) according to the standard protocol. RT-qPCR was conducted on the QuantStudio™ 7 Flex System using one step PrimeScript® RT-PCR Kit (Takara, RR064 A, Tokyo, Japan). The primer sequences are as follows: FXR, forward primer, 5′-GCTTGATGT GCTACAAAAGCTG-3′, reverse primer, 5′-CGTGGT GATGGTTGAATGTCC-3′. FGF15, forward primer, 5′-GAG GACCAAAACGAACGAAATT-3′, reverse primer, 5′- ACG TCCTTGATGGCAATCG-3′. Myd88, forward 5′- TGTTCTTGAACCCTCGGACG-3′, reverse, 5′-CGAAAAGTTCCGGCGTTTGT-3′. CD45, forward 5′-GCTGATCTGGGACGTGAACA-3′, reverse, 5′- TTA TCCCCTTCTGATGCGCC-3′. ZO-1, forward 5′-TGA ACGTCCCTGACCTTTCG −3′, reverse, 5′- CTGTGG AGACTGCGTGGAAT −3′. IL-1β, forward 5′- TGCCAC CTTTTGACAGTGATG −3′, reverse, 5′- TTCTTGTGA CCCTGAGCGAC −3′. GAPDH, forward 5- CGTCCC GTAGACAAAATGGT-3′, reverse, 5′- GAATTTGCC GTGAGTGGAGT'. The amplification of Gapdh was utilized as an internal control. The relative mRNA expression was quantified by using the comparative CT (ΔCt) method and expressed as $2^{-\Delta\Delta Ct}$. All qRT-PCR experiments were repeated at least three times.

Fluorescence in situ hybridization

Intact intestinal segments containing faecal pellets were immersed in Metheca solution for 48 h, embedded in paraffin wax and cut into 3 μm thick sections. Paraffin sections of intact tissue with intestinal tract and intestinal contents slides were dewaxed at 60℃ for 10 min. The slides were soaked in xylene for two 10-min periods at 60℃, 100% Ethanol for 5 min, and in 95% ethanol for another 5 min. The sections were air-dried, and the paraffin was completely removed. The probe (5'-GCTGCCTCCCGTAGGAGT-3' conjugated with Alexa 546) was prepared in a 1:100 buffer dilution to form a hybridization solution. Pre-warmed 50 μl probe-hybridization solution was added to each section and incubated overnight at 50℃ in a humidity chamber. After the washing solution, the slides were washed with PBS for 10 min each time and sealed with DAPI, and photographed by a fluorescence microscope (Leica, Wetzlar, German).

Bile acid test

The bile acid profile in the study samples was analyzed by the BAP Ultra (Metabo-Profile, Shanghai, China), a bile acid detection kit provided by Metabo-Profile. Liver samples were homogenized, lysed in acetonitrile/methanol, centrifuged, lyophilized, rehydrated and the supernatant was extracted before being analyzed by ultra performance liquid chromatography tandem mass spectrometry (UPLC-MS/MS, ACQUITY UPLC-Xevo TQ-S, Waters Corp., Milford, MA, USA) for the quantitative determination of bile acids. The raw data files generated by UPLC-MS/MS are processed in MassLynx software (v4.1, Waters, Milford, MA, USA), which integrates each bile acid, creates a standard curve, and quantifies the process. Mass spectrometry-based quantitative metabolomics acquires actual concentrations by comparing metabolites in a sample of unknown concentration with a set of standards of known concentration (quantitative curve).

Statistics

All values are presented in the figures as mean ± SEM, with $^{*}P < 0.05$, $^{**}P < 0.01$, $^{***}P < 0.001$, $^{****}P < 0.0001$; n.s., no significance. The number of animals (n) utilized in the experiments is indicated in the figures. One dot represents one mouse or one section. The statistical differences were determined by unpaired, two-tailed Student's t-test for two-group comparisons. Moreover, differences between groups were compared using analysis of variance (ANOVA) test (normal) or Kruskal–Wallis test (non-normal). The survival rate was statistically analyzed by Mantel-Cox log-rank. Statistical charts and the data analysis were conducted using GraphPad Prism V.7.00 for Windows (GraphPad Software, San Diego, California, USA).

Supplementary Information

The online version contains supplementary material available at https://doi.org/10.1186/s12964-025-02224-w.

Supplementary Material 1

Supplementary Material 2

Supplementary Material 3

Supplementary Material 4

Supplementary Material 5

Acknowledgements
We thank Wuhan Senlan Biotechnology Co., Ltd. and Zhongke Yikang Biotechnology Co., Ltd. for providing 15 strains of probiotics for this study.

Data access
The data that supports the findings of this study are available in the supplementary material of this article. All materials and methods are also available in supplementary section.

Authors' contributions
QSW performed most of the experiments and drafted the manuscript. WXM and SZH partly contributed to the performance of CLP mice and sacrificed animals. WQ, LYL, HQH, and SHB contributed to managing the experimental mice and genotyping, and H&E staining. WJY and HCC contributed to analyzing the survival rates. LJQ and WZT provided critical revision of the manuscript. Cubero, WXR and LLJ contributed to supervising and reviewing the study. LLJ provided funding, study concept, design, analysis as well as critical revision. All authors agree with the accuracy or completeness of the manuscript, and the version to be released is finally approved.

Funding
This research was supported by grants from Pudong New Area Health Talent Training Program (2025PDWSYCBJ-04), Medical Innovation Research Special Project of Shanghai 2023 Science and Technology Innovation Action Plan (23Y11908300), the National Natural Science Foundation of China (82202401, 81971814, 8217010632), and the Shanghai Pujiang Program (2020PJD050).

Data availability
No datasets were generated or analysed during the current study.

Declarations

Ethics approval and consent to participate
The animal study was reviewed and approved by the Animal Protection and Utilization Committee of East Hospital affiliated with Tongji University.

Competing interests
The authors declare no competing interests.

Author details
[1]Department of Anesthesiology and Pain Management, School of Medicine, Yangpu Hospital, Tongji University, Shanghai 200090, China. [2]Department of Pain Management, School of Medicine, Shanghai East Hospital, Tongji University, Shanghai 200120, China. [3]Department of Pharmacy, School of Medicine, Ji'an Hospital, Shanghai East Hospital, Tongji University, Jiangxi 343006, China. [4]Clinical Center for Investigation, School of Medicine, Renji Hospital, Shanghai Jiao Tong University, Shanghai 200127, China. [5]Department of Anesthesiology, Ningbo First Hospital, Zhejiang 315010, China. [6]Department of Immunology, Ophthalmology and ENT, Complutense University School of Medicine, 28040 Madrid, Spain. [7]Institute of Pain Medicine, Shanghai East Hospital, School of medicine, Tongji University, Shanghai 200120, China.

Received: 16 March 2025 Accepted: 29 April 2025
Published online: 21 May 2025

References

1. Weng L, Xu Y, Yin P, Wang Y, Chen Y, Liu W, Li S, Peng JM, Dong R, Hu XY, et al. National incidence and mortality of hospitalized sepsis in China. Crit Care. 2023;27:84.
2. Otani S, Coopersmith CM. Gut integrity in critical illness. J Intensive Care. 2019;7:17.
3. Lelubre C, Vincent JL. Mechanisms and treatment of organ failure in sepsis. Nat Rev Nephrol. 2018;14:417–27.
4. Mittal R, Coopersmith CM. Redefining the gut as the motor of critical illness. Trends Mol Med. 2014;20:214–23.
5. Grosheva I, Zheng D, Levy M, Polansky O, Lichtenstein A, Golani O, Dori-Bachash M, Moresi C, Shapiro H, Del Mare-Roumani S, et al. High-Throughput Screen Identifies Host and Microbiota Regulators of Intestinal Barrier Function. Gastroenterology. 2020;159:1807–23.
6. Peck-Palmer OM, Unsinger J, Chang KC, Davis CG, McDunn JE, Hotchkiss RS. Deletion of MyD88 markedly attenuates sepsis-induced T and B lymphocyte apoptosis but worsens survival. J Leukoc Biol. 2008;83:1009–18.
7. McClave SA. Can feeding strategies alter immune signaling and gut sepsis in critical illness? JPEN J Parenter Enteral Nutr. 2021;45:66–73.
8. Wei Y, Yang J, Wang J, Yang Y, Huang J, Gong H, Cui H, Chen D. Successful treatment with fecal microbiota transplantation in patients with multiple organ dysfunction syndrome and diarrhea following severe sepsis. Crit Care. 2016;20:332.
9. Bauer M. The liver-gut-axis: initiator and responder to sepsis. Curr Opin Crit Care. 2022;28:216–20.
10. Di Ciaula A, Garruti G, Lunardi Baccetto R, Molina-Molina E, Bonfrate L, Wang DQ, Portincasa P. Bile Acid Physiology. Ann Hepatol. 2017;16(Suppl 1):S4–14.
11. He YJ, You CG. The Potential Role of Gut Microbiota in the Prevention and Treatment of Lipid Metabolism Disorders. Int J Endocrinol. 2020;2020:8601796.
12. Tang L, Tang Z. Progress in the pathogenesis of cholestasis during the early stage of sepsis. Zhonghua Wei Zhong Bing Ji Jiu Yi Xue. 2021;33:506–8.
13. Geiger SS, Traba J, Richoz N, Farley TK, Brooks SR, Petermann F, Wang L, Gonzalez FJ, Sack MN, Siegel RM. Feeding-induced resistance to acute lethal sepsis is dependent on hepatic BMAL1 and FXR signalling. Nat Commun. 2021;12:2745.
14. Albillos A, de Gottardi A, Rescigno M. The gut-liver axis in liver disease: Pathophysiological basis for therapy. J Hepatol. 2020;72:558–77.
15. Gadaleta RM, van Erpecum KJ, Oldenburg B, Willemsen EC, Renooij W, Murzilli S, Klomp LW, Siersema PD, Schipper ME, Danese S, et al. Farnesoid X receptor activation inhibits inflammation and preserves the intestinal barrier in inflammatory bowel disease. Gut. 2011;60:463–72.
16. Kim MS, Shigenaga J, Moser A, Feingold K, Grunfeld C. Repression of farnesoid X receptor during the acute phase response. J Biol Chem. 2003;278:8988–95.
17. Gadaleta RM, Oldenburg B, Willemsen EC, Spit M, Murzilli S, Salvatore L, Klomp LW, Siersema PD, van Erpecum KJ, van Mil SW. Activation of bile salt nuclear receptor FXR is repressed by pro-inflammatory cytokines activating NF-κB signaling in the intestine. Biochim Biophys Acta. 2011;1812:851–8.
18. Vavassori P, Mencarelli A, Renga B, Distrutti E, Fiorucci S. The bile acid receptor FXR is a modulator of intestinal innate immunity. J Immunol. 2009;183:6251–61.
19. Fay KT, Klingensmith NJ, Chen CW, Zhang W, Sun Y, Morrow KN, Liang Z, Burd EM, Ford ML, Coopersmith CM. The gut microbiome alters immunophenotype and survival from sepsis. FASEB J. 2019;33:11258–69.
20. Liao L, Schneider KM, Galvez EJC, Frissen M, Marschall HU, Su H, Hatting M, Wahlstrom A, Haybaeck J, Puchas P, et al. Intestinal dysbiosis augments liver disease progression via NLRP3 in a murine model of primary sclerosing cholangitis. Gut. 2019;68:1477–92.
21. Wang C, Li Q, Ren J. Microbiota-Immune Interaction in the Pathogenesis of Gut-Derived Infection. Front Immunol. 1873;2019:10.
22. Pandey GN, Rizavi HS, Bhaumik R, Ren X. Innate immunity in the postmortem brain of depressed and suicide subjects: Role of Toll-like receptors. Brain Behav Immun. 2019;75:101–11.
23. Natividad JM, Hayes CL, Motta JP, Jury J, Galipeau HJ, Philip V, Garcia-Rodenas CL, Kiyama H, Bercik P, Verdu EF. Differential induction of antimicrobial REGIII by the intestinal microbiota and Bifidobacterium breve NCC2950. Appl Environ Microbiol. 2013;79:7745–54.

24. Lacroix-Lamandé S, Guesdon W, Drouet F, Potiron L, Lantier L, Laurent F. The gut flora is required for the control of intestinal infection by poly(I:C) administration in neonates. Gut Microbes. 2014;5:533–40.
25. Fu J, Wang T, Xiao X, Cheng Y, Wang F, Jin M, Wang Y, Zong X. Clostridium Butyricum ZJU-F1 Benefits the Intestinal Barrier Function and Immune Response Associated with Its Modulation of Gut Microbiota in Weaned Piglets. Cells. 2021;10:527.
26. Renga B, Mencarelli A, Cipriani S, D'Amore C, Carino A, Bruno A, Francisci D, Zampella A, Distrutti E, Fiorucci S. The bile acid sensor FXR is required for immune-regulatory activities of TLR-9 in intestinal inflammation. PLoS ONE. 2013;8: e54472.
27. Duparc T, Plovier H, Marrachelli VG, Van Hul M, Essaghir A, Stahlman M, Matamoros S, Geurts L, Pardo-Tendero MM, Druart C, et al. Hepatocyte MyD88 affects bile acids, gut microbiota and metabolome contributing to regulate glucose and lipid metabolism. Gut. 2017;66:620–32.
28. Kuzmich NN, Sivak KV, Chubarev VN, Porozov YB, Savateeva-Lyubimova TN, Peri F. TLR4 Signaling Pathway Modulators as Potential Therapeutics in Inflammation and Sepsis. Vaccines. 2017;5:34.
29. Rittirsch D, Huber-Lang MS, Flierl MA, Ward PA. Immunodesign of experimental sepsis by cecal ligation and puncture. Nat Protoc. 2009;4:31–6.
30. Fu J, Zang Y, Zhou Y, Chen C, Shao S, Hu M, Shi G, Wu L, Zhang D, Zhang T. A novel triptolide derivative ZT01 exerts anti-inflammatory effects by targeting TAK1 to prevent macrophage polarization into pro-inflammatory phenotype. Biomed Pharmacother. 2020;126: 110084.
31. Kim SJ, Baek KS, Park HJ, Jung YH, Lee SM. Compound 9a, a novel synthetic histone deacetylase inhibitor, protects against septic injury in mice by suppressing MAPK signalling. Br J Pharmacol. 2016;173:1045–57.
32. Al-Shahwani NH, Sigalet DL. Pathophysiology, prevention, treatment, and outcomes of intestinal failure-associated liver disease. Pediatr Surg Int. 2017;33:405–11.
33. Garcia-Irigoyen O, Moschetta A. A Novel Protective Role for FXR against Inflammasome Activation and Endotoxemia. Cell Metab. 2017;25:763–4.
34. Hao H, Cao L, Jiang C, Che Y, Zhang S, Takahashi S, Wang G, Gonzalez FJ. Farnesoid X Receptor Regulation of the NLRP3 Inflammasome Underlies Cholestasis-Associated Sepsis. Cell Metab. 2017;25:856-867.e855.
35. Madnawat H, Welu AL, Gilbert EJ, Taylor DB, Jain S, Manithody C, Blomenkamp K, Jain AK. Mechanisms of Parenteral Nutrition-Associated Liver and Gut Injury. Nutr Clin Pract. 2020;35:63–71.
36. Rafferty JF, Noguchi Y, Fischer JE, Hasselgren PO. Sepsis in rats stimulates cellular proliferation in the mucosa of the small intestine. Gastroenterology. 1994;107:121–7.
37. Meng M, Klingensmith NJ, Liang Z, Lyons JD, Fay KT, Chen CW, Ford ML, Coopersmith CM. Regulators of Intestinal Epithelial Migration in Sepsis. Shock. 2019;51:88–96.
38. Di Cerbo A, Palmieri B, Aponte M, Morales-Medina JC, Iannitti T. Mechanisms and therapeutic effectiveness of lactobacilli. J Clin Pathol. 2016;69:187–203.
39. Brownlie EJE, Chaharlangi D, Wong EO, Kim D, Navarre WW. Acids produced by lactobacilli inhibit the growth of commensal Lachnospiraceae and S24–7 bacteria. Gut Microbes. 2022;14:2046452.
40. Keighley MR, Burdon DW, Cooke WT, Slaney G, Alexander W. Proceedings: The importance of bacteroides as a cause of severe sepsis after colorectal surgery. Gut. 1975;16:408.
41. Wexler HM. Bacteroides: the good, the bad, and the nitty-gritty. Clin Microbiol Rev. 2007;20:593–621.
42. Niu M, Chen P. Crosstalk between gut microbiota and sepsis. Burns Trauma. 2021;9:tkab036.
43. Essex M, Millet Pascual-Leone B, Löber U, Kuhring M, Zhang B, Brüning U, Fritsche-Guenther R, Krzanowski M, Fiocca Vernengo F, Brumhard S, et al. Gut microbiota dysbiosis is associated with altered tryptophan metabolism and dysregulated inflammatory response in COVID-19. NPJ Biofilms Microbiomes. 2024;10:66.
44. Li W, Chen H, Tang J. Interplay between Bile Acids and Intestinal Microbiota: Regulatory Mechanisms and Therapeutic Potential for Infections. Pathogens. 2024;13:702.
45. Larabi AB, Masson HLP, Bäumler AJ. Bile acids as modulators of gut microbiota composition and function. Gut Microbes. 2023;15:2172671.
46. Anderson KM, Gayer CP. The Pathophysiology of Farnesoid X Receptor (FXR) in the GI Tract: Inflammation Barrier Function and Innate Immunity. Cells. 2021;10:3206.
47. Zhou X, Cao L, Jiang C, Xie Y, Cheng X, Krausz KW, Qi Y, Sun L, Shah YM, Gonzalez FJ, et al. PPARalpha-UGT axis activation represses intestinal FXR-FGF15 feedback signalling and exacerbates experimental colitis. Nat Commun. 2014;5:4573.
48. Yang JY, Liu MJ, Lv L, Guo JR, He KY, Zhang H, Wang KK, Cui CY, Yan BZ, Du DD, et al. Metformin alleviates irradiation-induced intestinal injury by activation of FXR in intestinal epithelia. Front Microbiol. 2022;13: 932294.
49. Wildenberg ME, van den Brink GR. FXR activation inhibits inflammation and preserves the intestinal barrier in IBD. Gut. 2011;60:432–3.
50. Yan M, Hou L, Cai Y, Wang H, Ma Y, Geng Q, Jiang W, Tang W. Effects of Intestinal FXR-Related Molecules on Intestinal Mucosal Barriers in Biliary Tract Obstruction. Front Pharmacol. 2022;13: 906452.
51. Jian YP, Yang G, Zhang LH, Liang JY, Zhou HL, Wang YS, Xu ZX. Lactobacillus plantarum alleviates irradiation-induced intestinal injury by activation of FXR-FGF15 signaling in intestinal epithelia. J Cell Physiol. 2022;237:1845–56.
52. Lainšček D, Horvat S, Dolinar K, Ivanovski F, Romih R, Pirkmajer S, Jerala R, Manček-Keber M. MyD88 protein destabilization mitigates NF-κB-dependent protection against macrophage apoptosis. Cell Commun Signal. 2024;22:549.
53. Guo Q, Jin Y, Chen X, Ye X, Shen X, Lin M, Zeng C, Zhou T, Zhang J. NF-κB in biology and targeted therapy: new insights and translational implications. Signal Transduct Target Ther. 2024;9:53.
54. Li H, Xie J, Guo X, Yang G, Cai B, Liu J, Yue M, Tang Y, Wang G, Chen S, et al. Bifidobacterium spp and their metabolite lactate protect against acute pancreatitis via inhibition of pancreatic and systemic inflammatory responses. Gut Microbes. 2022;14:2127456.
55. Wennekamp J, Henneke P. Induction and termination of inflammatory signaling in group B streptococcal sepsis. Immunol Rev. 2008;225:114–27.
56. Schneider KM, Candels LS, Hov JR, Myllys M, Hassan R, Schneider CV, Wahlstrom A, Mohs A, Zuhlke S, Liao L, et al. Gut microbiota depletion exacerbates cholestatic liver injury via loss of FXR signalling. Nat Metab. 2021;3:1228–41.
57. Stadlbauer V, Horvath A, Komarova I, Schmerboeck B, Feldbacher N, Klymiuk I, Durdevic M, Rainer F, Blesl A, Stiegler P, Leber B. Dysbiosis in early sepsis can be modulated by a multispecies probiotic: a randomised controlled pilot trial. Benef Microbes. 2019;10:265–78.
58. Zanza C, Romenskaya T, Thangathurai D, Ojetti V, Saviano A, Abenavoli L, Robba C, Cammarota G, Franceschi F, Piccioni A, Longhitano Y. Microbiome in Critical Care: An Unconventional and Unknown Ally. Curr Med Chem. 2022;29:3179–88.
59. Khailova L, Frank DN, Dominguez JA, Wischmeyer PE. Probiotic administration reduces mortality and improves intestinal epithelial homeostasis in experimental sepsis. Anesthesiology. 2013;119:166–77.
60. Shimizu K, Yamada T, Ogura H, Mohri T, Kiguchi T, Fujimi S, Asahara T, Yamada T, Ojima M, Ikeda M, Shimazu T. Synbiotics modulate gut microbiota and reduce enteritis and ventilator-associated pneumonia in patients with sepsis: a randomized controlled trial. Crit Care. 2018;22:239.
61. Lou X, Xue J, Shao R, Yang Y, Ning D, Mo C, Wang F, Chen G. Fecal microbiota transplantation and short-chain fatty acids reduce sepsis mortality by remodeling antibiotic-induced gut microbiota disturbances. Front Immunol. 2022;13:1063543.
62. Sanaie S, Ebrahimi-Mameghani M, Hamishehkar H, Mojtahedzadeh M, Mahmoodpoor A. Effect of a multispecies probiotic on inflammatory markers in critically ill patients: A randomized, double-blind, placebo-controlled trial. J Res Med Sci. 2014;19:827–33.
63. Zheng Y, Zhang Z, Tang P, Wu Y, Zhang A, Li D, Wang CZ, Wan JY, Yao H, Yuan CS. Probiotics fortify intestinal barrier function: a systematic review and meta-analysis of randomized trials. Front Immunol. 2023;14:1143548.
64. Kwoji ID, Aiyegoro OA, Okpeku M, Adeleke MA. Multi-Strain Probiotics: Synergy among Isolates Enhances Biological Activities. Biology (Basel). 2021;10:322.
65. Iskander KN, Craciun FL, Stepien DM, Duffy ER, Kim J, Moitra R, Vaickus LJ, Osuchowski MF, Remick DG. Cecal ligation and puncture-induced murine sepsis does not cause lung injury. Crit Care Med. 2013;41:159–70.
66. Dejager L, Pinheiro I, Dejonckheere E, Libert C. Cecal ligation and puncture: the gold standard model for polymicrobial sepsis? Trends Microbiol. 2011;19:198–208.

Publisher's Note

Springer Nature remains neutral with regard to jurisdictional claims in published maps and institutional affiliations.